UNDERSTANDING ION TRANSPORT MECHANISM IN IONIC DEVICES FROM A MOLECULAR LEVEL

A Dissertation

Presented to the Faculty of the Graduate School

of Cornell University

in Partial Fulfillment of the Requirements for the Degree of

Master of Science

by

Jinyue Dai

August 2023

UNDERSTANDING ION TRANSPORT MECHANISM IN IONIC DEVICES FROM A MOLECULAR LEVEL

Jinyue Dai

Cornell University 2023

Soft ionic materials combine charged mobile species and tailored polymer structures in a manner that enables a wide array of functional devices. Ionic devices hold the promise of using the wide range of chemical and molecular properties of mobile ions and polymer functional groups to enable flexible conductors, deformable digital or analog signal processors, which have emerged as promising candidates for various applications in energy storage, electronic sensing, and biomedical devices. Central to their functionality is the intricate ion transport mechanism that governs the movement of charged species within their structures. This thesis delves into the fundamental understanding of ion transport mechanisms in ionic devices, unraveling the intricacies from a molecular level. Molecular dynamics simulations are employed to investigate the behavior of ions within two ionic devices, metal-ligand coordinated polymeric conductors and polyelectrolyte diodes, shedding light on the factors influencing their mobility and diffusion such as clustering, hopping or water content. By bridging the gap between theoretical insights and experimental observations, this work provides a molecular level understanding on the underlying ion transport mechanism and the relationship between the device performance.

Keywords: ion transport, ionic devices, molecular dynamics, ionic clustering, ionic conductivity, rectification effect

ACKNOWLEDGEMENTS

I am deeply grateful to everyone who has contributed to the completion of this master thesis, as their support and encouragement have been invaluable throughout this arduous yet rewarding journey.

First and foremost, I extend my utmost gratitude to my esteemed supervisor, Meredith Silberstein, for their unwavering guidance, patience, and expertise. Their insightful feedback and constant encouragement have been instrumental in shaping the direction of this research and have pushed me to strive for excellence in every aspect of my work.

I would like to express my appreciation to my committee member, Jingjie Yeo, for dedicating their time and expertise in reviewing my research and providing valuable insights that have strengthened the quality of this thesis.

I am deeply indebted to my collaborators and lab mates who graciously volunteered their time and shared their valuable insights, without whom this study would not have been possible. Their willingness to be a part of this research has enriched its depth and significance.

In conclusion, this thesis stands as a testament to the collective efforts and support of all those mentioned above, as well as those whose names might not be written here but whose influence on my journey has been no less significant. I dedicate this work to all who have played a part in shaping my academic and personal growth.

TABLE OF CONTENTS

Acknowledgements 4
Table of Contents 5
List of Tables 6
List of Figures 7

1 Introduction **1**

2 Metal-ligand coordinated polymer **5**
2.1 Methods 7
2.1.1 Molecular dynamics simulation setup and equilibration . 7
2.1.2 Clustering and ionic conductivity analysis 10
2.1.3 Ion hopping analysis 13
2.1.4 Transference number 13
2.1.5 Viscosity 14
2.2 Results and Discussion 15
2.2.1 The effect of metal-ligand coordination 15
2.2.2 The effect of counter anions 24
2.2.3 The effect of ion concentration 29
2.2.4 The effect of cation identity 30

3 Polyelectrolyte Diode **35**
3.1 Methods 38
3.1.1 Simulation details 38
3.1.2 Static ionic conductivity 40
3.2 Results and Discussion 43
3.2.1 Dry polymer 43
3.2.2 Polyelectrolyte gel 44

4 Conclusions and Future Directions **48**

A Appendix 1 **52**

LIST OF TABLES

2.1 Atomic point charges for LiOTf[1] 8
2.2 Atomic point charges for LiTFSi[2] 8

LIST OF FIGURES

2.1 (a-f) Cluster analysis of **P-PI/LiOTf1** with cutoff distance from 2.4 Å to 3.4 Å with an increment of 0.2 Å. n_+ and n_- is the number of cations and anions composing of each cluster, respectively. α_{ij} is the average count of each cluster over the simulation period. . 12

2.2 Comparison between the model and control systems. The chemical structure and schematic of (a) the LiOTf coordinated PDMS, **P-PI/LiOTf1**; (b) the mixture of pristine PDMS and LiOTf, **P-NH_2/LiOTf1**. Schematics show the expected different degree of cation-anion dissociation in the PDMS with and without ligand functionalization. 17

2.3 MD simulation setup and results. (a) Schematic representation of different Li^+ coordination environments within **P-PI/LiOTf1**. (b-d) Results of **P-PI/LiOTf1** and (e-g) results of **P-NH_2/LiOTf1**. (b, e) Coordination matrix that presents the relative contribution to the total coordination of Li^+ by oxygens from OTf^- and nitrogens from the end groups of the polymer chains. The grid squares passed through by the red and yellow line represents the most favorable total coordination numbers of 4 and 5. p_{ij} is the probability of each coordination combination over the simulation time. (c, f) MSD plot of cations, anions and polymer chains. (d, g) Ion clustering statistics, where the grid squares passed through by the red line represents the neutral clusters. α_{ij} is the average count of each cluster over the simulation period. 20

2.4 Coordination matrix of Li^+ from (a) the siloxanes and ligands; (b) the anions and siloxanes for **P-PI/LiOTf1**. 22

2.5 Radial distribution function of Li^+ surrounded by siloxane oxygen for **P-PI/LiOTf1**. 23

2.6 Variation over time of atom indices coordinating a less diffusive lithium atom for **P-PI/LiOTf1**. 24

2.7 Variation over time of atom indices coordinating a more diffusive lithium atom for **P-PI/LiOTf1**. 25

2.8 Variation over time of atom indices coordinating a specific lithium atom for **P-NH_2/LiOTf1**. 25

2.9 Variation over time of atom indices coordinating a specific lithium atom for **P-PI/LiOTf2**. 26

2.10 MD simulation results for **P-PI/LiTFSi1**. (a) Coordination matrix; (b) MSD plot of mobile species; (c) ion clustering statistics. . 28

2.11 Li^+ coordinated PDMS. (a) A comparison of diffusion coefficients from both experimental and simulation results: diffusion coefficients of ^1H from PDMS chain and ^{19}F from counter anions in Li salts are obtained from PFG SE NMR measurements at 100 °C, and diffusion coefficients of Li^+ and counter anions are obtained from MD simulation at 100 °C. Error bars are calculated from ^1H in different moieties on the PDMS chain; (b) Ionic conductivity of LiOTf and LiTFSi coordinated PDMS with varying salt concentration.[3] 30
2.12 MSD plot of mobile species and cluster analysis for (a) **P-PI/LiOTf0.4**; (b) **P-PI/LiOTf1**; (c) **P-PI/LiOTf2.0**. 31
2.13 Cu^{2+} coordinated PDMS. (a) The chemical structure of **P-PI/Cu(OTf)$_2$1** predicted from the mass spectrum; (b) Frequency sweeps at a strain of 0.1% measured by rheology, with sample photos of **P-PI/Cu(OTf)$_2$1** and **P-PI/LiOTf1**;[3] (c) The variation of ionic conductivity of the polymer.[3] 32
2.14 MD simulation results for **P-PI/Cu(OTf)$_2$1**. (a) Ion clustering statistics; (b) coordination matrix; (c) MSD plots of mobile species; (d) variation over time of atom indices coordinating a specific copper ion. 34

3.1 The chemical structure of PDADMA and PSS 37
3.2 (a) The setup of the diode simulation; (b) The schematic of the whole system (left) and ions only (right) after forward bias. . . . 39
3.3 (a) Electric field; (b) electrostatic potential; (c) partial density; (d) charge distribution with respect to the average relative position from center across the lateral dimension (z) of the box. t_0 is at equilibrium, t_f is after forward bias and t_r is after reverse bias. . . 42
3.4 MSD of the translation dipole moment versus time for (a) simulations under different initial conditions. Sim1 demonstrates that the forward bias directly start after equilibrium and Sim2 demonstrates that the forward bias follows an initial reverse bias. Inset copied from Cayre et al[4]. (b) forward bias under different electric field strengths. 45
3.5 MSD of the translation dipole moment versus time for dry and wet diodes under forward and reverse bias at 0.02 V/nm 46
3.6 The steady state or switching time analysis for diodes. σ is the ionic conductivity under forward bias, where dry diode is at 0.1 V/nm and wet diode is at 0.02 V/nm. 47

CHAPTER 1

INTRODUCTION

Ion-conducting polymers are a class of materials that exhibit the ability to transport ions, typically cations or anions, through their polymeric matrix. These polymers have attracted significant attention due to their unique combination of mechanical flexibility, ease of processing, and ionic conductivity. The field of ion-conducting polymers dates back several decades, with early research focused on solid polymer electrolytes for batteries and fuel cells.[5, 6] Over time, advancements in polymer chemistry and materials engineering have led to the development of a wide range of ion-conducting polymers, with varying structures, compositions, and properties. For example, most of the pioneering studies on polymer electrolytes are based on polyethylene oxide (PEO) complexed with alkali metal salts.[7, 8] Ionic liquids have been either mixed into neutral polymer networks or polymerized into poly(ionic liquid)s (PILs) for engineering various electrochemical devices.[9, 10] Ionic polymer metal composites (IPMC) consisting of a polyelectrolyte membrane placed in between two noble metal electrodes have been studied to enable large actuation under an applied electric field.[11] Continued effort has been made to both develop novel ionically conductive polymers and understand fundamental ion conducting mechanisms, to enable rational design based on functional requirements for a particular application.

As the palette of multifunctional polymers continues to grow, researchers have begun imagining how they could be used to create an entirely new class of functional devices such as energy storage, electrochemical devices, sensors, and actuators.[12–16]. The past 100 years have been marked by the dramatic

development and proliferation of electronics. However, electrical conductors are generally limited to electrons (and sometimes holes) as their current carrying particles, and are typically rigid. Ionic conductors can take advantage of the wide array of ions. A single wire could carry many ion signals simultaneously, or interact directly with the ionic signalling found throughout nature. Ionic materials promise to usher in a new era of ionic devices that are more biocompatible, biointerfacing, flexible, and low-power than electronics. The developments necessary to realize fully ionic devices are occurring in many fields simultaneously, while the building blocks share similar fundamental science. Molecular dynamics (MD) simulations have emerged as a powerful tool for better understanding the behavior and properties of ionic polymeric materials and devices at the atomic and molecular level.[17–21] By simulating the motion and interactions of individual atoms or molecules over time, they enable researchers to explore the structural dynamics, transport mechanisms, and thermodynamic properties of materials, providing valuable insights that are often challenging to obtain through experimentation alone.

One essential function within a device is to move information from point A to point B. Movement of mobile ions in response to an external stimuli allows for signal transmission across a soft ionic polymer. In ionic devices, this information takes the form of electric fields and chemical concentrations. The most common ionic device responsible for signal transmission in an ionic circuit is ionic conductors. The signal transmission through ionic conductors can rely on different or multiple mechanisms: hopping, vehicular, diffusion or Grotthuss,[16] which are the physics that underpin the magnitude of the ion mobility coefficient. For example, hydrogels and ionogels can be good ionic conductors. Conductivity in these systems can be on the order of 1 $S m^{-1}$,[22] but generally

decreases with increasing crosslink density,[23] resulting in a tradeoff between mechanical and ionic transport properties. Metal-ligand coordinated polymers are another class of high performance ionic conductors with tunable dynamics junctions. The strength of the metal-ligand coordination and ion correlation can lead to the simultaneous enhancement of conducting and mechanical properties.[24–26] Some other ionic conductors are highly deformable with excellent self-healing properties. [27–29]

Almost all ionically conducting polymers can act as a resistor, which is an element that has a linear relationship between the electrochemical potential difference between two places and the ion current that flows between those two places. In addition to the linear element, analog circuits often take advantage of nonlinear elements. The most common of these is the ionic diode. A polycation, with mobile counter anions, behaves similarly to an n-doped semiconductor, which has mobile negatively charged electrons. A polyanion, with mobile counter cations, behaves similarly to a p-doped semiconductor. When a polycation and polyanion are touched to each other, they form a bipolar membrane, which is a junction that behaves like a diode. There are also other nonlinear elements like the ionic capacitors, which can be made by inverting the structure of an electrolytic or super capacitor,[30, 31] or the ionic transistors including bipolar junction transistors[32–34]and field effect transistors[35, 36].

Besides those elements mentioned above, a lot of other ionic devices are invented for the integration of ionic circuits, for example, sensors and actuators,[37–40] energey sources like the flexible batteries,[41] reverse electrodialysis,[42] mechanical ion transducers[43] and ionic thermoelectrics[44] and so on. However, there is still a gap between ion transport or interaction

and macroscopic device behavior. To invent more complex circuits, the atomic or molecular level understanding on individual device is valuable and necessary. This thesis uses MD simulations to provide insights into strategic design of ionic devices, specifically 1) metal-ligand coordinated ionic conductor and 2) polyelectrolyte diode. We discuss the fundamental mechanisms for ion movement, and how it is related to the improvement of the electrical and mechanical properties of ionic devices. We believe our work will facilitate a deeper understanding of the structure-property relationships in ionic materials, guiding the design and synthesis of advanced ionic devices.

CHAPTER 2

METAL-LIGAND COORDINATED POLYMER

Ion mobility and ion concentration are the two key factors governing ionic conductivity of a polymer; the former is not only directly related to the identity and quantity of cations and anions, but is also greatly affected by the physical and chemical characteristics of the polymer matrix bearing the ions.[45] Polymers with low glass transition temperature and low crystallinity are good candidates to achieve high ionic conductivity at room temperature for practical applications.[46] However, polyelectrolytes predominantly have high polarity backbones to facilitate ion dissociation, which raises the glass transition temperature or promotes crystallinity by increasing intermolecular interactions.[47] In contrast, polymers with low dielectric constants, like PDMS, have low glass transition temperatures and maintain an amorphous state, but are barely ionically conductive due to poor salt dissociation.[48] Metal-ligand coordination as a non-covalent interaction has been extensively applied in polymer matrices to enhance the mechanical toughness, tune viscoelasticity, and enable self-healing.[49–54] In recent years, metal-ligand coordination has also been studied as a means of designing ionically conductive polymers.[24, 26, 55, 56] For example, imidazole-and imidazolium-containing polymers, which can bind with metals, have been synthesized and studied.[57, 58] This moiety is particularly interesting due to its wide prevalence in nature and in the human body, and is therefore relevant in bioactive applications.[57] In addition, polymer electrolytes containing metal-ligand coordination such as Li^+ coordinated poly(N-methyl-malonic amide) and Zn^{2+} coordinated polyacrylamide have been developed for all-solid-state batteries.[59, 60]

It is vital to build fundamental understanding of the ion conducting mechanisms of these amorphous, elastomeric, metal-coordinated polymers, and the relation of these mechanisms to the polymer structure. Molecular dynamics (MD) simulations are a powerful approach to provide detailed insight into transport phenomenon in ionic polymeric materials at the atomistic level.[19, 61] So far, MD simulations related to ionic conductivity have mainly focused on collecting single ion dynamics. Ionic conductivity is commonly determined with the Nernst-Einstein (NE) equation, which gives conductivity as directly proportional to the diffusion coefficients of the ions. The NE approximation works well for dilute systems with high dielectric constants, but fails in the concentrated ion regime.[18, 62] An alternative approach by Wheeler and Newman, following a Green-Kubo methodology in the Stephan-Maxwell framework, reported large noise for determining off-diagonal transport coefficients.[63] Grossman et al. proposed the cluster Nernst Einstein (cNE) method that accounts for salt nucleation.[2] They showed that their method could reproduce the experimental results of PEO-based electrolytes at high salt loading.[2] Their method should be also applicable to other cases with solvent-free or low dielectric constant, where the capacity to dissociate ion pairs is relatively weak and therefore the ions form clusters.

In this study, we combine fully atomistic MD simulations with in-depth experimental studies to unveil ion conducting mechanisms in metal-coordinated PDMS. A low molecular weight polydimethylsiloxane (PDMS) end-functionalized with pyridyl imine ligands is selected as the model system, and a series of Li and Cu salts are added to form polymer complexes. Factors that govern the ionic conductivity of the material, including ion dissociation, ion concentration, and chain mobility, are discussed in the context of the

metal-ligand coordination density and strength. Firstly, we highlight that the formation of metal-ligand coordination promotes salt dissociation into ions and therefore enhances the ionic conductivity of the PDMS complex as compared to the direct mixing of pristine PDMS and metal salt. Next, we show that the choice of counter anion, and ion concentration can vary the ionic conductivity of PDMS by orders of magnitude due to the distinct cation-anion interactions. Furthermore, we propose and prove that the mechanical strength can be greatly improved with different metal cation choice. To elucidate the ion transport mechanisms, a range of properties are computed from the MD simulations, including the ion and polymer chain diffusion coefficients, ionic conductivity, and salt clustering.

2.1 Methods

2.1.1 Molecular dynamics simulation setup and equilibration

The fully atomistic MD simulations are performed with the Large Atomic Molecular Massive Parallel Simulator (LAMMPS). Each simulated system consists of 20 PDMS chains, each with 21 monomers long, 20 salt pairs are doped into the system for PDMS:salt = 1 : 1 case. For each salt species, we considered 9 randomized trajectories from 3 different initial configurations and 3 different initial velocity seeds to average out the noise.[64]

Force field parameters and initial configurations for the PDMS and ions are generated with the Enhanced Monte Carlo (EMC) software [65] using the polymer-consistent force field (PCFF) [66]. The point charge assigned to the

ion pairs is rescaled by 0.7 (Table **??**). The charge downscale procedure is commonly used for classical force fields where a static point-charge model can lead to an exaggeration of ionic interaction strength.[67] More accurate electrostatics could be described by applying polarizable charge equilibration model [68] or polarizable force field [69] but either would lead to a dramatic increase in computational costs.

Table 2.1: Atomic point charges for LiOTf[1]

Species	Charge(e)
Li	0.7000
S	0.4481
C	0.4200
F	−0.1120
O	−0.4107

Table 2.2: Atomic point charges for LiTFSi[2]

Species	Charge(e)
Li	0.7000
S	0.4480
C	0.4200
F	−0.1120
O	−0.2940
N	−0.5880

The velocity-Verlet integrator with a time step of 0.5 fs is used for motion evolution; this value is selected as the largest one ensuring reasonable drift of atoms within a single time step. The relaxation process consists of steepest descent and conjugate gradient energy minimization, followed by equilibration in

the canonical (nVT) and isothermal-isobaric (nPT) statistical ensembles at the target temperature and pressure of 303 K and 1 bar, for a total duration of 5 ns. The Nose-Hoover thermostats and barostats are used with damping parameters set to 50 and 500 fs, respectively. The production run is conducted in the nVT ensemble at 303 K for 50 ns, except for the diffusion coefficient comparison with experimental results that was conducted at 373 K. For non-bonded interactions, long-range electrostatic interactions are calculated by using the particle-particle particle-mesh solver with a 1.2 nm cutoff distance while Lennard-Jones interactions are truncated at 1.2 nm with the long-range Van der Waals tail corrections included for energy and pressure modification.

Most force fields for transition metal complexes are based on either 1) treating the coordination bonds as covalent bonds with known maximum connectivity of each atom; or 2) treating the interaction between the transition metal and ligands as nonbonded interactions consisted of the electrostatic (Columbic) and van der Waals (VDW) energy terms, with transition metal ion treated as ions bearing formal charge. We have implemented both of the above force field models in MD simulations. Based on the pair-wise cutoff distance criteria, the covalent bonds are created between pairs of atoms with the maximum number of bonds each atom can have being manually set. It is found out that the one with permanent covalent bonds lacks the information about accurate bond formation or dissociation. Once the bond formed, it would be permanently in place. The most common connectivity of copper metal atoms can range from 4-8, depending on the allowed maximum connectivity. For the second approach, the coordination bonds are dissociative but too dynamic to represent the transition metal-ligand complex structure. The most common coordination matrix is found to be $2N_{Py}$–$4O_{OTf}$ or $4N_{Py}$–$2O_{OTf}$.

To describe the interaction between the copper metal atom and nitrogen atoms of the ligands, we use the partial charge model to made a potential function [70], which is consisted of two parts: the Morse function for covalence contribution and the Columbics for electrostatic contribution:

$$U_{bond(metal-ligand)} = A[(1 - exp^{-B(r_{ij}-C)})^2 - 1] + \frac{q_i q_j}{r_{ij}} \tag{2.1}$$

The model is parameterized well fitting the QM data with AMBER force field. We further evaluate the effect of the Cu^{2+} coordination strength using a toy model with scaled parameters in PCFF, where A is 47.84, B is 1.109 and C is 2.004. The simulation setup is similar with that of the lithium system, except for the hybrid overlay of the potential functions as mentioned above.

2.1.2 Clustering and ionic conductivity analysis

The self-diffusion coefficient is calculated using the Einstein relation:

$$D_{ion} = \lim_{t\to\infty} \frac{\left\langle \frac{1}{N} \sum_{i=1}^{N} |\mathbf{x}_i(t_0 + t) - \mathbf{x}_i(t_0)|^2 \right\rangle_{c,t_0}}{6t} \tag{2.2}$$

where $\mathbf{x}_i(t)$ is the instantaneous position of i^{th} particle at time t and N is the number of particles. The numerator is mean-squared displacement (MSD) of a molecule center of mass during time t and $\langle ... \rangle$ denotes an ensemble average. Note that we performed both configuration averaging and time-origin averaging using a sliding-window strategy. The relation only holds for the Fickian regime of the MSD curve, therefore, it is necessary to reach the diffusive linear regime to extract an accurate diffusion coefficient. [71]

With the diffusion coefficients for mobile species obtained from MSD, we first calculate the ionic conductivity with the Nernst-Einstein equation, which

states that the total conductivity is proportional to individual diffusion coefficient and ionic concentration:

$$\sigma_{NE} = \frac{e^2}{Vk_BT}(N_+z^2{}_+D_+ + N_-z^2{}_-D_-) \tag{2.3}$$

where k_B is the Boltzmann constant, e is the elementary charge, V is the volume of simulation box, T is the temperature, $z_\pm$ and $N_\pm$ is the charge and number of cations and anions. However, the NE equation assumes ions do not interact with themselves, and is therefore only exact in the infinite dilution limit. For electrolytes with high salt concentrations, ionic transport shifts from single free charge carriers to clusters of salt nucleating, which has the primary function of scaling down the conductivity by forming neutral clusters. To account for the effect of clustering, Grossman et al. reformulated the Nernst-Einstein equation with the assumption that clusters do not interact with each other: [2]

$$\sigma_{cNE} = \frac{e^2}{Vk_BT}\sum_{i=0}^{N_+}\sum_{j=0}^{N_-} z^2{}_{ij}\alpha_{ij}D_{ij} \tag{2.4}$$

where the fundamental charge carriers are no longer single free ions but ionic clusters of different charge numbers $z_{ij} = iz_+ + jz_-$. α_{ij} is the matrix element that defines the population of the cluster consisting of i cations and j anions, which is averaged over ensembles and long simulation time. D_{ij} is the diffusion coefficient for each type of cluster, written in matrix form. Cation(s) and anion(s) are defined to belong to the same cluster if the cation is within the cutoff distance of one or more of the anions. It is worth noting that neutral clusters with $z_{ij} = 0$ do not contribute to the total conductivity although they do also diffuse. This is the first time that the cluster Nernst-Einstein (cNE) has been applied to polymer-in-salt systems other than PEO or PEO-based variants.[72]

To correlate the ionic conductivity, we implement the cluster analysis with MD simulations, where cation(s) and anion(s) are defined to be part of the same

cluster if the cation is within the cutoff distance from one or more atoms of the anions. The cutoff distance is chosen to be 2.8 Å for LiOTf and 3.25 Å for LiTFSi. The choice for the cutoff distance of the cluster analysis is not unique: a lower threshold value would artificially increase the number of free Li atoms and OTf^-/$TFSi^-$ molecules while a higher threshold would increase the fraction of larger clusters (Figure 2.1). Importantly, the qualitative features of the cluster population are conserved with varied cutoff distances, which is also proved by Molinari et al. [18]

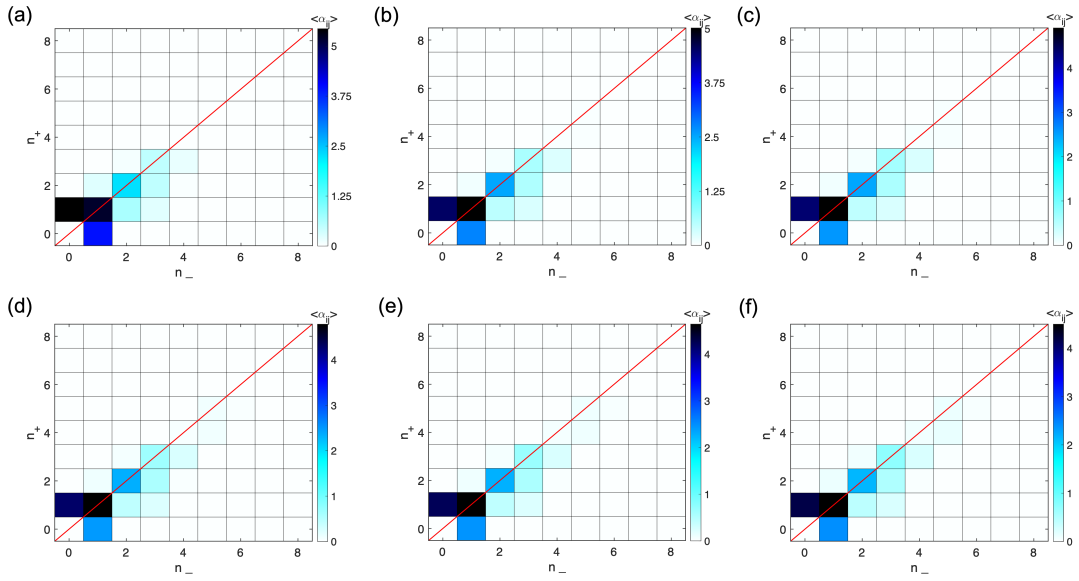

Figure 2.1: (a-f) Cluster analysis of **P-PI/LiOTf1** with cutoff distance from 2.4 Å to 3.4 Å with an increment of 0.2 Å. n_+ and n_- is the number of cations and anions composing of each cluster, respectively. α_{ij} is the average count of each cluster over the simulation period.

2.1.3 Ion hopping analysis

The ion hopping analysis is characterized by tracking the coordination environment change of one single ion. Specifically, ion hopping can be monitored by tracking the location and corresponding residence time that a single ion spends with some atoms on specific polymer chains. Time-dependent trajectory of cation coordination is traced based on a distance criterion (i.e., an atom contributes to the coordination of a cation when its distance to the cation is less than the coordination cutoff). In our case, the coordination from the most electronegative nitrogen atoms of the polymer chains and the oxygen atoms of the anions are tracked over the simulation time. The consecutive indices correspond to consecutive coordination from the same chain or anion, while the switch between two different consecutive lines, indicates a cation jump among chains.

2.1.4 Transference number

The transference number from MD simulations is calculated with cluster Nernst Einstein (cNE) approach, which accounts the clustering effect for ion transport: [2]

$$t^{+}_{cNE} = \frac{\sum_{i=0}^{N_+} \sum_{j=0}^{N_-} i z_+ z_{ij} \alpha_{ij} D_{ij}}{\sum_{i=0}^{N_+} \sum_{j=0}^{N_-} {z^2}_{ij} \alpha_{ij} D_{ij}} \tag{2.5}$$

where i is the number of cations in cluster ij. In contrast to most experimental transference number measurement methods, this definition of the transference number allows the possibility of a negative t^{+}_{cNE} because the numerator can be negative. A negative value would be a side effect of clustering, with the cations being drawn to the anode through correlation with the anions. A neg-

ative transference number has also been reported experimentally [73–75] and computationally[2, 76] in recent years.

2.1.5 Viscosity

The shear viscosity is a kinetic property which is useful for parameterizing the force field. Several methods for determining the shear viscosity are available from MD simulations.[77] There are two equilibrium methods based on pressure or momentum fluctuations and a few nonequilibrium molecular dynamics (NEMD) methods. Here, we focus on the pressure fluctuation-based equilibrium method and the commonly used SLLOD algorithm for steady-state shear.[78]

The viscosity can be calculated from an equilibrium simulation by integrating the Green-Kubo formula:[79]

$$\eta = \frac{V}{k_B T} \int_0^\infty \left\langle P_{\alpha\beta}(t_0) P_{\alpha\beta}(t_0 + t) \right\rangle \, dt \tag{2.6}$$

where η is the viscosity, V is the box volume, k_B is the Boltzmann constant, T is the temperature, $P_{\alpha\beta}$ is an off-diagonal component of the stress tensor, and t is time. The function $\left\langle P_{\alpha\beta}(t_0) P_{\alpha\beta}(t_0 + t) \right\rangle$ is an autocorrelation function with the average taken over all time origins and off-diagonal components ($\alpha\beta$ is yz, xz or xy). The viscosity of **P-PI/LiOTf1** from equilibrium simulation is about 3.6 *cst*. We confirm that the equilibrium method can result in poorly converged viscosities and the value of viscosity heavily depends on the sampling frequency, correlation length and plateau point (integration time), which causes inaccuracies.[80]

Instead of measuring the intrinsic fluctuations of the system, which have a

fixed magnitude, one can also obtain the viscosity by imposing a Couette flow. With sliding boundary conditions, each point in the simulation would have a position-dependent streaming velocity, which does not contribute to the thermal temperature of the atom. The viscosity is calculated from the stress tensor **P**:

$$\eta = -\frac{1}{s}\left\langle P_{\alpha\beta}\right\rangle \tag{2.7}$$

where s is the shear rate. The viscosity of **P-PI/LiOTf1** is about 16 cst with a shear rate of $10^9/s$. For NEMD, imposed deformations often happen too fast, where the shear strain rates are unrealistically high and temperature quenches are orders of magnitudes faster than experiment. [81] For the purpose of quick and accurate convergence, we choose NEMD to calculate the viscosity of different systems for this research.

2.2 Results and Discussion

2.2.1 The effect of metal-ligand coordination

To understand how metal-ligand coordination promotes the ionic conductivity of a polymer, we choose low molecular weight PDMS as the polymer precursor because of its many advantageous features. First, PDMS has a low glass transition temperature ($T_g \approx -123$ °C), yielding dynamic chain motion at room temperature, which facilitates the transport of ions.[82, 83] Second, PDMS has low inherent ion impurity content[84] and low dielectric constant ($\kappa \approx 2.3 - 2.8$)[85], which serves as a non-conductive baseline and creates a clear contrast in the ionic conductivity of the polymer before and after introducing metal-ligand co-

ordination. Furthermore, ion interaction in the system is mainly mediated by the metal-ligand coordination rather than the solvation of polymer backbone, which offers us a good model to decouple the effect of metal-ligand coordination from other factors that contribute to the ionic conductivity.[48, 86] Third, PDMS has many good physical and chemical properties such as being stretchable and inert. Finally, PDMS is easy to fabricate and low cost, which makes it a popular material candidate for next-generation ionic devices.[16, 87]

We create a model system by functionalizing the ends of low molecular weight PDMS with a metal coordinating ligand. Pyridyl imine is selected as the functional group because it is a versatile ligand that can coordinate with various metal cations.[88] The model system (**P-PI**, P represents PDMS, PI represents pyridyl imine ligand) is synthesized via a condensation reaction between aminopropyl terminated PDMS (**P-NH_2**, NH_2 represents amine end group) and 2-pyridinecarboxaldehyde.[89] The structure of **P-PI** is confirmed by ^{1}H NMR with a number average molecular weight (M_n) of around 2000 g/mol. The dielectric constant for **P-NH_2** of this molecular weight is measured experimentally to be 3.3, with a slight decrease to 3.1 for **P-PI**.

To study how the formation of coordination complexes affects the ionic conductivity of the model system, a monovalent metal cation Li^+ is added. Since Li^+ has a coordination number of $4-6$ with different ligand molecules, it is important to determine the coordination stoichiometry between Li^+ and the pyridiyl imine ligand.[90, 91] Therefore, a small-molecule model ligand, N-propyl(2-pyridyl)methanimine, is synthesized, and is combined with lithium trifluoromethanesulfonate (LiOTf) salt to form a small-molecule Li^+-pyridyl imine complex. The experimental mass spectrum of this complex indicates that

the ratio between Li^+ and pyridyl imine ligand is 1 : 2.[3] Since pyridyl imine groups are present at the both ends of the PDMS chain, this number implies that the ligands are fully coordinated with Li^+ when the molar ratio of PDMS to LiOTf is 1 : 1.

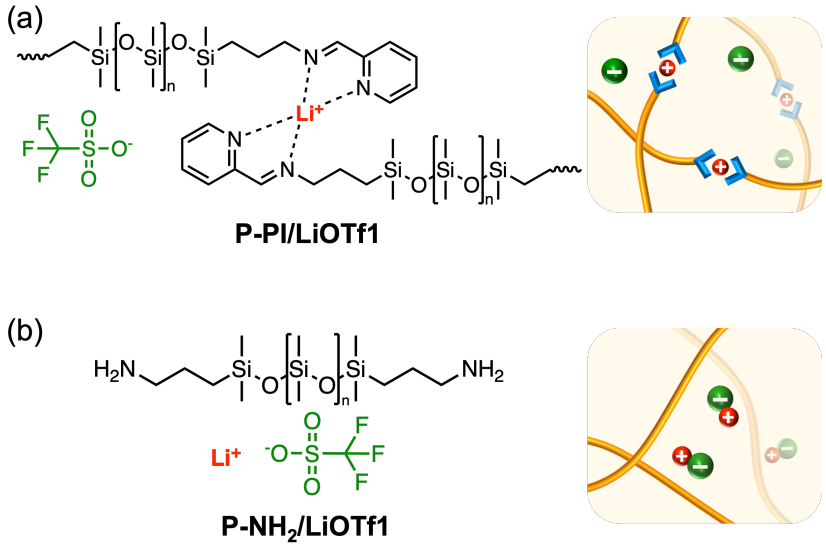

Figure 2.2: Comparison between the model and control systems. The chemical structure and schematic of (a) the LiOTf coordinated PDMS, **P-PI/LiOTf1**; (b) the mixture of pristine PDMS and LiOTf, **P-NH_2/LiOTf1**. Schematics show the expected different degree of cation-anion dissociation in the PDMS with and without ligand functionalization.

Next, a polymer complex with this 1 : 1 molar ratio of pyridyl imine functionalized PDMS to LiOTf is synthesized (**P-PI/LiOTf1**, Figure 2.2a). Two additional polymers are used as controls: (1) **P-PI** with no LiOTf salt, and (2) pristine PDMS mixed with same quantity of LiOTf salt (**P-NH_2/LiOTf1**, Figure 2.2b). The formation of a complex between the PDMS and Li^+ is verified by Fourier-transform infrared spectroscopy (FTIR). The ionic conductivity of the model and controls is measured using electrochemical impedance spectroscopy (EIS): **P-PI** has an extremely low ionic conductivity that is below the limit of de-

tection because of the low ion impurity content ($\sigma < 4.8 \times 10^{-10}\ S/m$); in contrast, the ionic conductivity of **P-PI/LiOTf1** increases by at least 5 orders of magnitude, yielding the value of $(4.28 \pm 0.22) \times 10^{-5}\ S/m$.[3] Although **P-NH$_2$/LiOTf1** also shows improved ionic conductivity ($\sigma = (2.51 \pm 0.12) \times 10^{-6}\ S/m$) compared to the pure PDMS, it is only about 6% of the value of **P-PI/LiOTf1**. Since the same amount of LiOTf salt is added into the PDMS with and without ligand functionalization, we infer that the extent of salt ionization determines the ionic conductivity of the material.[86] The significantly higher ionic conductivity of **P-PI/LiOTf1** compared to **P-NH$_2$/LiOTf1** demonstrates that the formation of metal-ligand coordination facilitates cation-anion dissociation and therefore improves the ionic conductivity of the PDMS.

To provide critical molecular level insights that are hard to capture by experimental characterization techniques, fully atomistic molecular dynamics (MD) simulations are performed with LAMMPS (Figure 2.3a).[92] The molecular interaction is described using PCFF framework.[66] Each simulated system consists of 20 PDMS chains, each 21 monomers long, and 20 LiOTf molecules, equivalent to the experimentally characterized structure. Results for the MD simulated **P-PI/LiOTf1** and **P-NH$_2$/LiOTf1** are given in Figure 2.3b-d and Figure 2.3e-g, respectively.

With the equilibrated MD system, we first compare the polymer-salt interaction in **P-PI/LiOTf1** and **P-NH$_2$/LiOTf1**. From the coordination matrices shown in Figure 2.3b and Figure 2.3e, Li^+ tends to interact with different electronegative moieties in the two system. In **P-PI/LiOTf1**, Li^+ has a strong tendency to coordinate both with the nitrogen atom on the pyridyl imine group and the oxygen atoms on OTf^-. In **P-NH$_2$/LiOTf1**, Li^+ preferably interacts with the oxygen

atoms on OTf^-. It is worth noting that the most favorable lithium coordination is 4 and 5, consistent with previous work by Olsher et al.[93] The geometries of most 4-fold coordination and 5-fold coordination structures are found to be close to tetrahedral and square-pyramidal by visualization with Visual Molecular Dynamics (VMD)[94] software. In addition, the coordination matrix in Figure 2.4 indicates that Li^+ barely interacts with the siloxane group on the PDMS backbone. The coordination analysis based on simulation is consistent with our mass spectroscopy experimental results, confirming that the most probable structure is 4-fold coordination, which helps to validate the transferability of the PCFF force field to the PDMS and salt system.

To better understand the effect of metal-ligand coordination on ion and chain mobility, we investigate the diffusion coefficient of different components in the MD simulations of these two material systems. The MSD plots of ions and polymer chains for **P-PI/LiOTf1** are shown in Figure 2.3c. Both Li^+ and OTf^- motion is subdiffusive before 5 ns, i.e., $MSD \propto \tau^{\alpha}$ with $\alpha < 1$. At times longer than 5 ns, the ion motion becomes diffusive and the diffusion coefficient can be obtained from the MSD by applying the Einstein relation (Equation (2.2)). The OTf^- diffusion coefficient ($D_{OTf^-} = 1.12$ Å$^2/ns$) is larger than the Li^+ diffusion coefficient ($D_{Li^+} = 0.84$ Å$^2/ns$). These results show that both cations and anions are mobile in the polymer matrix, with anions having higher mobility than cations. We infer that the motion of cations is mainly through the ligand exchange process, and is slowed down by this transient coordination interaction; in contrast, anions are less confined and the motion is facilitated by chain segmental motion. The PDMS (**P-PI**) chains also diffuse over time, but at a substantially slower rate than the ions. For **P-NH$_2$/LiOTf1**, the MSD curves of cations and anions (Figure 2.3f) almost coincide, with similar diffusion coefficients of $D_{Li^+} = 2.75$ Å$^2/ns$

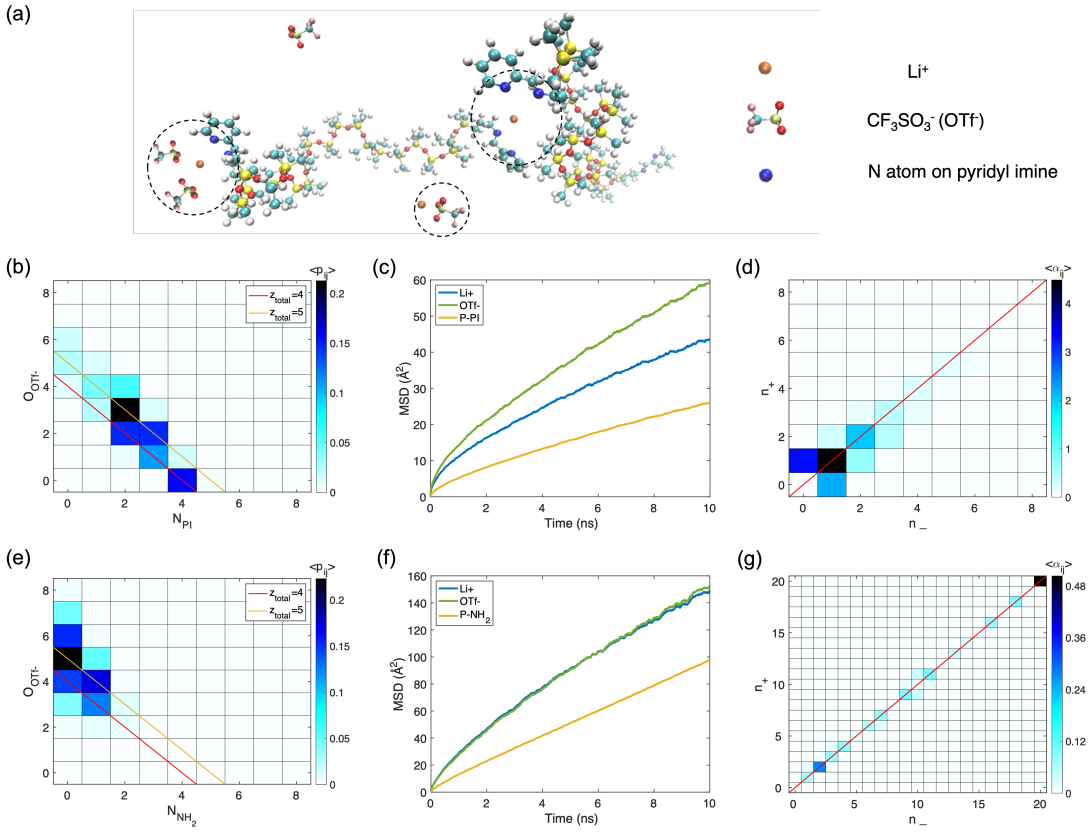

Figure 2.3: MD simulation setup and results. (a) Schematic representation of different Li^+ coordination environments within **P-PI/LiOTf1**. (b-d) Results of **P-PI/LiOTf1** and (e-g) results of **P-NH$_2$/LiOTf1**. (b, e) Coordination matrix that presents the relative contribution to the total coordination of Li^+ by oxygens from OTf^- and nitrogens from the end groups of the polymer chains. The grid squares passed through by the red and yellow line represents the most favorable total coordination numbers of 4 and 5. p_{ij} is the probability of each coordination combination over the simulation time. (c, f) MSD plot of cations, anions and polymer chains. (d, g) Ion clustering statistics, where the grid squares passed through by the red line represents the neutral clusters. α_{ij} is the average count of each cluster over the simulation period.

and $D_{OTf^-} = 2.78$ Å$^2/ns$). This is due to the poor solvation ability of pristine PDMS, which promotes the formation of ionic clusters and results in the cations and anions diffusing together. Interestingly, the diffusion coefficients of both

the ions and the chains in **P-NH$_2$/LiOTf1** are about three times larger than their values in **P-PI/LiOTf1**, resulting from the fact that ion motion in **P-NH$_2$/LiOTf1** encounters less confinement from the PDMS chains due to minimal coordination. At first glance, this seems contrary to the experimental results since ionic conductivity is typically thought to be directly related to the diffusion coefficient. However, the presence of ionic clusters instead of single ions significantly decreases the quantity of charge carriers in the system, and therefore yields low ionic conductivity of the material.

Ion clustering is a common phenomenon at high salt concentration or when the interaction with the local structure is not strong enough for salt ionization, leading to correlated motion of cations and anions.[95] According to the cluster Nernst-Einstein (cNE) approach developed by Grossman et al., the net charge and diffusivity of each ionic cluster are aggregated to give the overall system conductivity (i.e. neutral clusters do not contribute to conductivity, Equation (2.4)).[2] The cluster populations of **P-PI/LiOTf1** and **P-NH$_2$/LiOTf1** are shown in Figures 2.3d and 2.3g, respectively. For **P-PI/LiOTf1**, both charged clusters and neutral clusters are observed at thermodynamic equilibrium, with clusters composed of up to 12 ions (6 cations and 6 anions). For **P-NH$_2$/LiOTf1**, the cluster analysis shows an increase of cluster size, up to all the ions in the simulation box (into a single cluster). The formation of very bulky neutral ionic clusters explains the lower ionic conductivity compared to that of **P-PI/LiOTf1** measured from experiments. More importantly, it demonstrates that by introducing ligands onto the polymer chains, the formation of metal-ligand coordination reduces large neutral ionic aggregation and facilitates the transport of charge carriers, improving the conductivity. Using the cNE equation (Equation (2.4)), we find conductivity for **P-PI/LiOTf1** is $0.0041\ S/m$ while that for **P-NH$_2$/LiOTf1** is

0.00036 S/m. The ratio of the ionic conductivity with ligands to without is about 11.4 times, which matches well with the ratio of 17 from the experiments. Without the cluster correction on the NE equation, the ionic conductivity would be 0.036 S/m and 0.11 S/m for **P-PI/LiOTf1** and **P-NH$_2$/LiOTf1**, which would contradict the experimental results. We note here that while our trends match well with experiments, our predicted conductivity values are substantially above the experimentally measured values. We believe this has to do with the scaled representation of the cation-anion interaction strength, which will be discussed in more depth when we compare results for different anions.

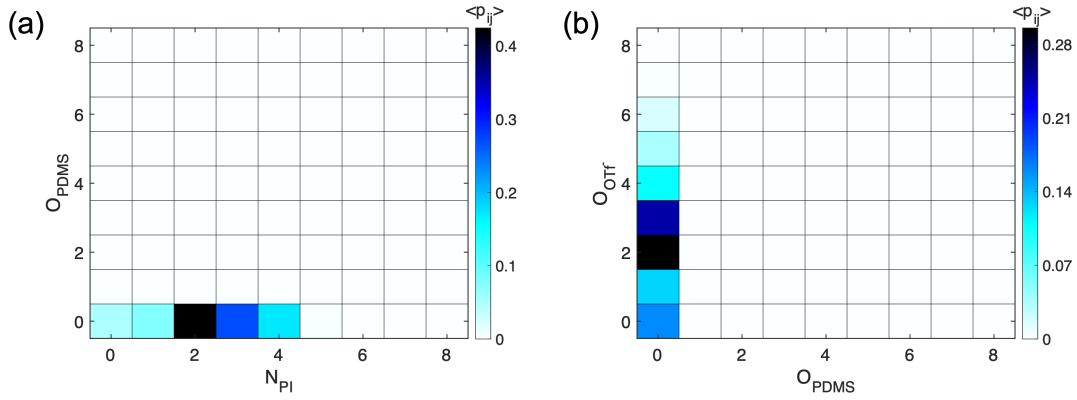

Figure 2.4: Coordination matrix of Li^+ from (a) the siloxanes and ligands; (b) the anions and siloxanes for **P-PI/LiOTf1**.

Next, we are interested in assessing whether interchain cation hopping via continuous ligand exchange is an important transport mechanism for cations. We suspect cation hopping might be important, because the MSD plots show that chain motion is 2-3 times slower than Li^+ diffusion, indicating that cation diffusion, on this timescale, is not solely driven by the segmental motion of the polymer. The hopping behavior varies considerably among individual cations. In Figure 2.6 and Figure 2.7 we show the behavior of two example ions: the less diffusive Li^+ tends to attach to one ligand from one chain over the entire

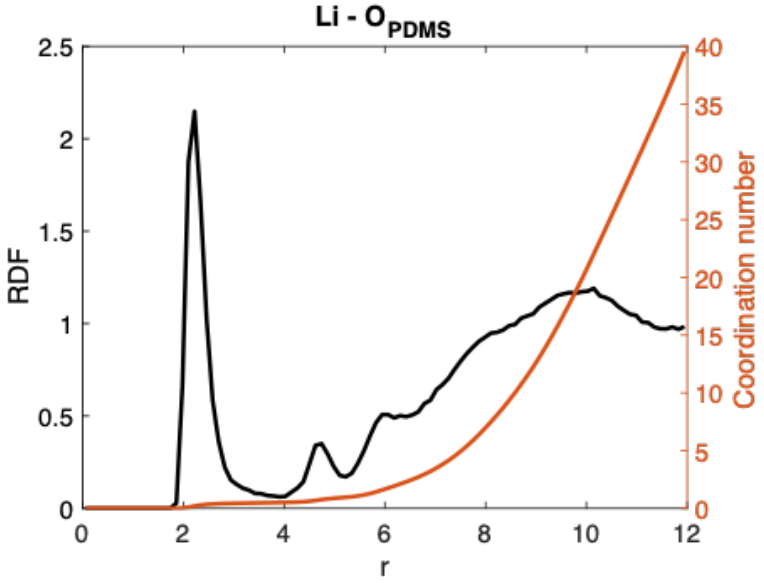

Figure 2.5: Radial distribution function of Li^+ surrounded by siloxane oxygen for **P-PI/LiOTf1**.

80 *ns* simulated while exchanging among other ligands from different chains; the more diffusive Li^+ hops frequently between chains. It is shown in Figure 2.8 that Li^+ jumping among polymer chains is more frequent in **P-NH$_2$/LiOTf1** than in **P-PI/LiOTf1**, due to the weak polymer-ion interaction and hence short residence time when there is no ligand. It is also found that Li^+ tends to coordinate with one single chain while constantly exchange the rest coordination with other ligands. In addition, the motion of Li^+ along the host chain is insignificant for this material system, contrary to other polymer-salt systems like PEO electrolytes,[96] because only the ligand grafted on the ends of the chains can coordinate with the lithium ions, while the monomers hardly interact with Li^+ due to the non-polar nature of PDMS. The coordination matrix and radial distribution function (RDF) plot of oxygens within the PDMS backbone relative to the lithium ions supports this lack of association, showing an average coordination number of zero (Figure 2.4, 2.5).Furthermore, we find that higher ion

concentration can lead to more frequent ligand exchange by comparing Figure 2.7 and Figure 2.9.

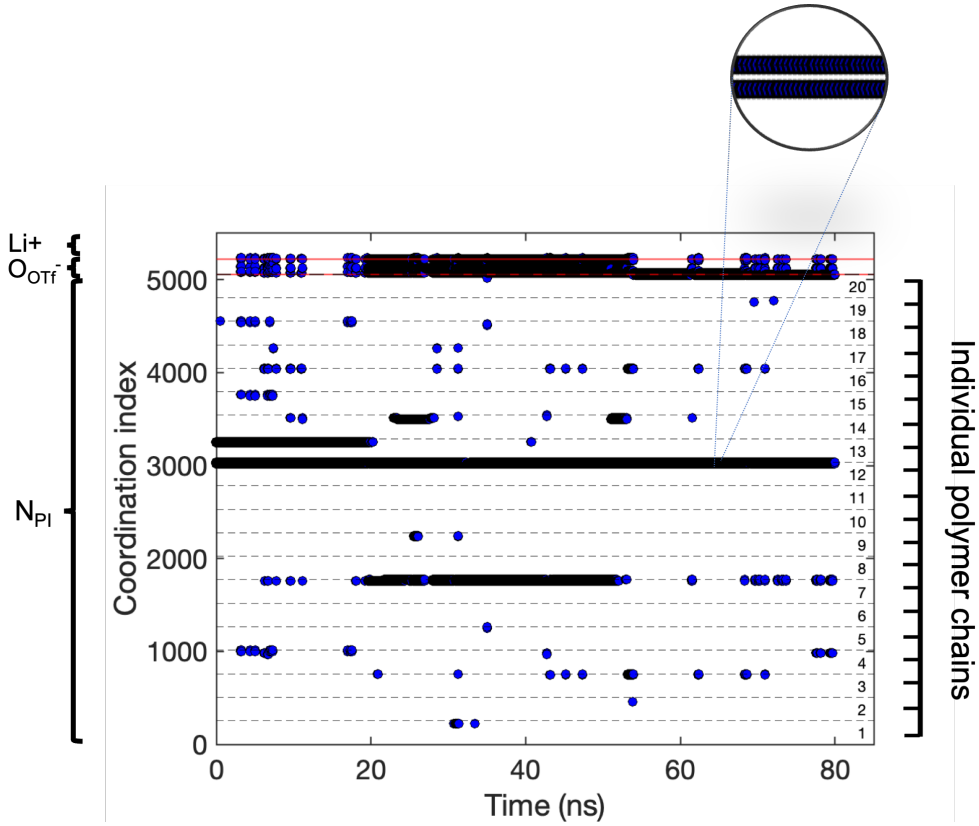

Figure 2.6: Variation over time of atom indices coordinating a less diffusive lithium atom for **P-PI/LiOTf1**.

2.2.2 The effect of counter anions

Since varying the counter anion in a metal-ligand complex can yield distinct coordination strength and lifetime, a series of Li^+ coordinated PDMS with different anion species is synthesized to study the influence of counter ions on ionic conductivity.[54, 97] The ionic conductivity of the Li^+ coordinated PDMS with different counter anions is measured by EIS and shows orders of magnitude differences: **P-PI/LiCl1** < **P-PI/LiBF$_4$1** < **P-PI/LiOTf1** < **P-PI/LiTFSi1**.[3]

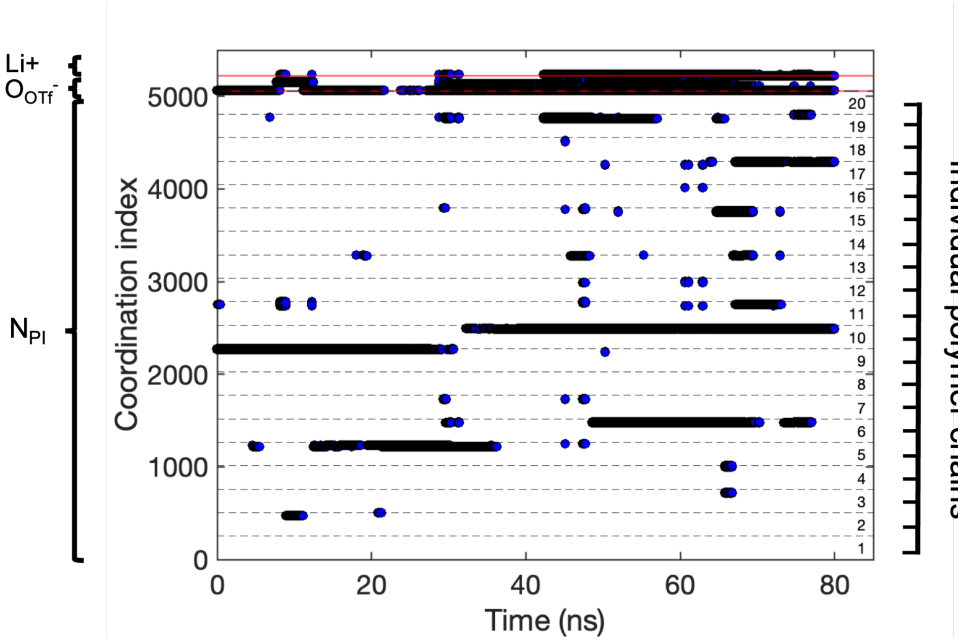

Figure 2.7: Variation over time of atom indices coordinating a more diffusive lithium atom for **P-PI/LiOTf1**.

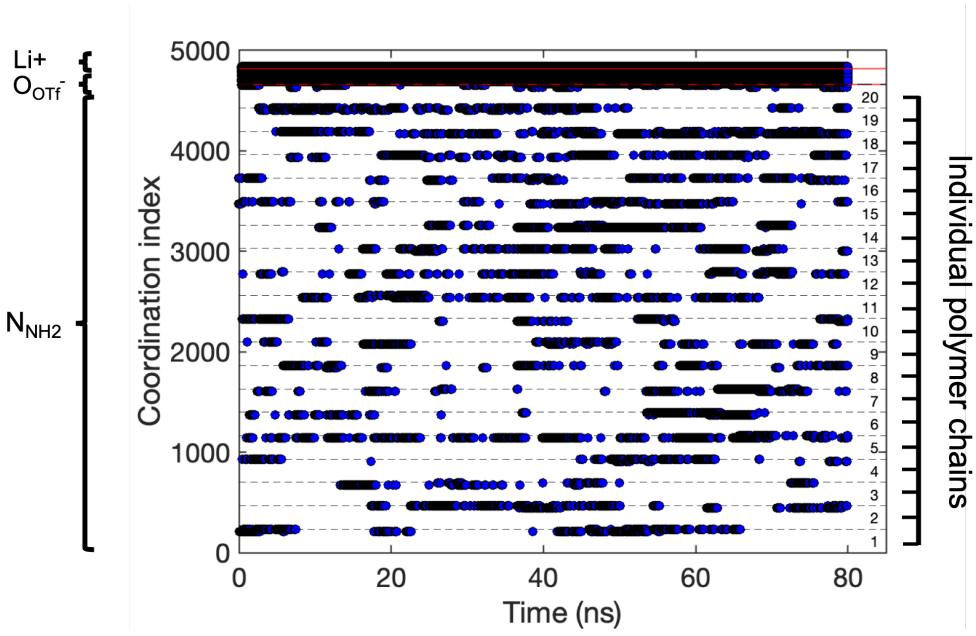

Figure 2.8: Variation over time of atom indices coordinating a specific lithium atom for **P-NH_2/LiOTf1**.

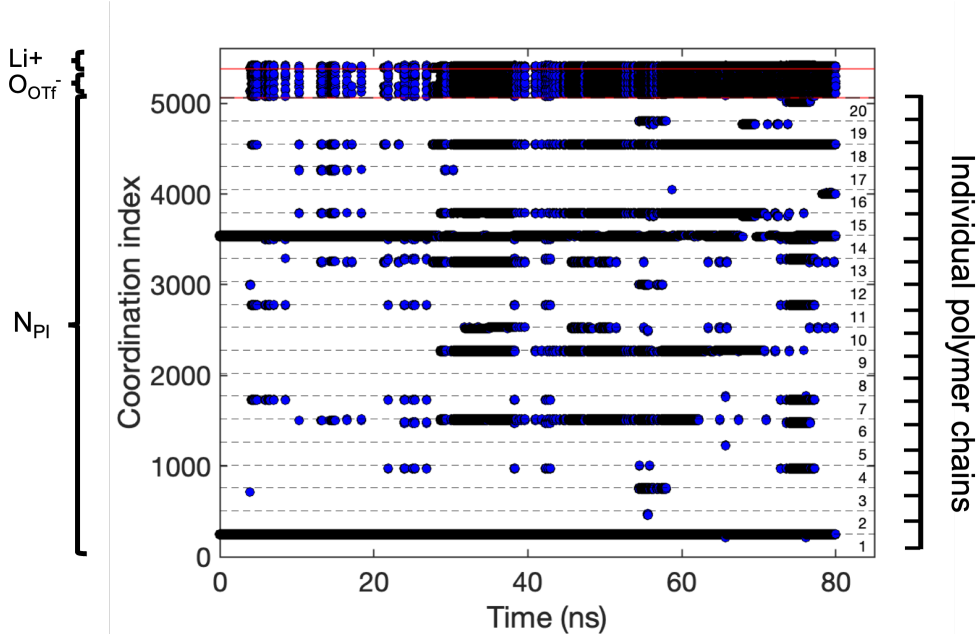

Figure 2.9: Variation over time of atom indices coordinating a specific lithium atom for **P-PI/LiOTf2**.

The ionic conductivity of the Li^+ coordinated PDMS increases with the size of the counter anion. Bulkier counter anions such as OTf^- and $TFSi^-$ have higher charge delocalization, yielding weaker cation-anion interaction, and therefore the increased ion mobility promotes higher ionic conductivity.[86] The MD simulations of **P-PI/LiTFSi1** also show greater ionic conductivity than **P-PI/LiOTf1** ($\sigma_{TFSi^-} = 0.0054\ S/m$ vs $\sigma_{OTf^-} = 0.0041\ S/m$), though the trend is less prominent than the experimental one. At 30 °C, the ionic conductivity from MD simulations for **P-PI/LiTFSi1** is about 3 times higher than the experimental value and it is about 46 times higher than the experimental value for **P-PI/LiOTf1**. The reason for the large discrepancy in **P-PI/LiOTf1** could be the underestimation of ionic correlation strength due to the use of a scaling charge factor, leading to greater diffusivity as molecular sizes decrease.

To gain a more quantitative insight into the mobility of the PDMS chain and

counter anions, the self-diffusion of the system is investigated in details. MD simulations of **P-PI/LiTFSi1** compared to **P-PI/LiOTf1** show that the bulkier, less polar $TFSi^-$ anion tends to have more frequent intercluster hopping, leading to an overall higher diffusivity ($D_{TFSi^-} = 1.66$ Å$^2/ns, D_{Li^+} = 1.26$ Å$^2/ns$). The cluster analysis from MD observations is provided in Figure 2.10, which is consistent with previous work on PEO-LiTFSi systems: there are mostly neutral ion pairs, but also a non-negligible concentration of negatively charged clusters, resulting in an overall asymmetric distribution.[72] The distribution of charged clusters in **P-PI/LiTFSi1** is less symmetric compared to that of **P-PI/LiOTf1**, with overall more negatively charged clusters present in the system, indicating that Li^+ from **P-PI/LiTFSi1** interacts more strongly with the polymer chains than Li^+ from **P-PI/LiOTf1**. Furthermore, the diffusion coefficients of positively charged clusters tend to be slightly smaller than those of negatively charged clusters with the same constituent number of ions, due to the stronger local interaction between positively charged clusters and electronegative ligands on the polymer.

The transference number calculated from MD simulations is 0.253 for **P-PI/LiOTf1** and -0.313 for **P-PI/LiTFSi1**. The positive transference number for **P-PI/LiOTf1** shows that the transport of cations or positively charged clusters dominates, while the negative transference number for **P-PI/LiTFSi1** confirms the existence of negatively charged clusters dominating the Li^+ transport. The Very Low Frequency EIS (VLFEIS) [98] transference number experimental measurements also shows that **P-PI/LiTFSI** has a much smaller transference number than **P-PI/LiOTf1** (0.07 vs 0.24) [3] which confirms that more of the current is carried by counter ions and negatively charged clusters in **P-PI/LiTFSI1** than in **P-PI/LiOTf1**. The discrepancy for the transference number of **P-PI/LiTFSi1**

between experiment and MD simulation can be due to 1) the reference frame gap [76] or 2) distinct assumptions of the simulation and experimental methods (clustering vs ideal electrolyte).[99] We attempted to close this methods gap by through Onsager transport coefficients from MD simulations, using the Wheeler-Newman expression. [63, 100]However, we found that noise led to highly variable off-diagonal transport coefficients across parallel simulations.

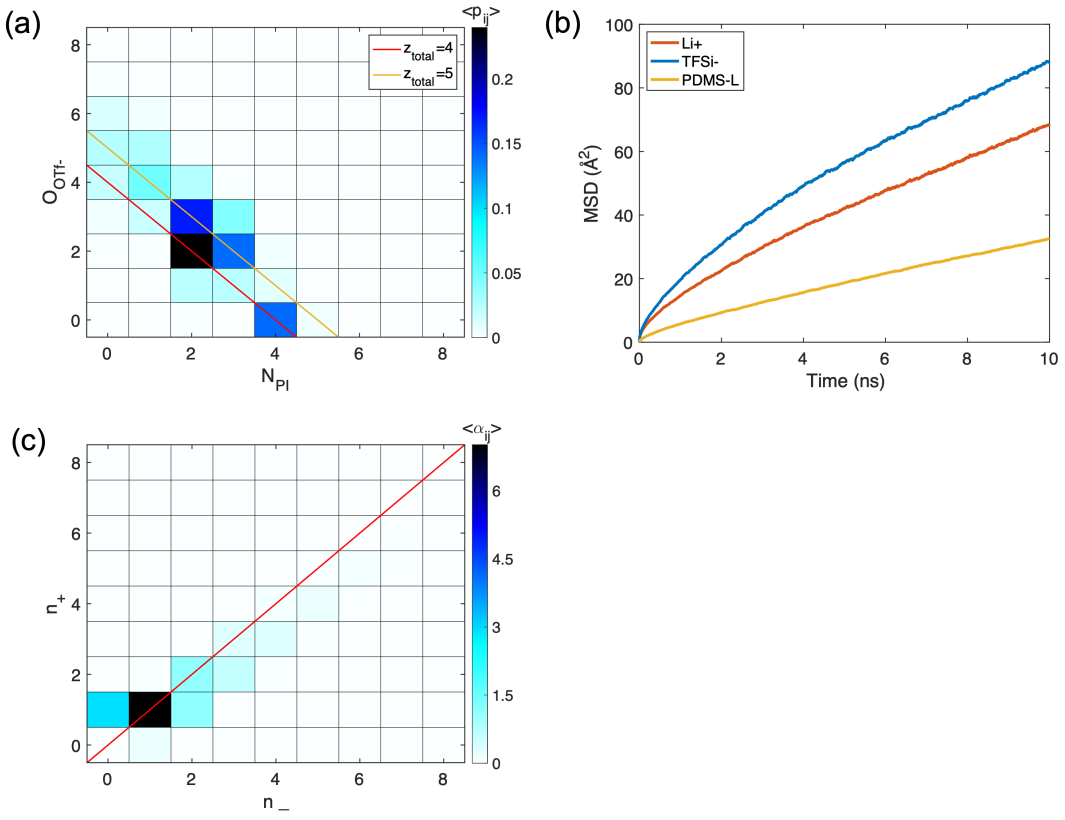

Figure 2.10: MD simulation results for **P-PI/LiTFSi1**. (a) Coordination matrix; (b) MSD plot of mobile species; (c) ion clustering statistics.

2.2.3 The effect of ion concentration

We study the effect of ion concentration on the ionic conductivity of the model system by preparing a series of LiOTf and LiTFSi coordinated PDMS with different salt concentrations (**P-PI/LiOTf0.2** to **P-PI/LiOTf1.4** and **P-PI/LiTFSi0.2** to **P-PI/LiTFSi1.4**, the number in the sample name indicates the molar ratio of PDMS:LiOTf = $1 : n$). In both cases, the ionic conductivity of the PDMS complex first increases and then decreases as the Li salt concentration increases; the highest ionic conductivity is reached at around the maximum coordination capacity of the ligands with Li^+ cations (corresponding to PDMS:Li salt = 1 : 1). This indicates that at first, more Li^+ cations and counter anions exist in the system as the Li salt concentration is increased, improving the ionic conductivity. However, when the ligand coordination capacity is oversaturated by excess Li salt, the ionic conductivity of the PDMS complex starts to decrease monotonically (Figure 2.11b). As both seen from the previous studies and our MD simulation (Figure 2.12), ion pairs and higher-order clusters form at high Li salt concentration, which hinders the effective cation-anion dissociation and ion transport, thereby decreasing the overall ionic conductivity.[18, 75, 101]

We can look more deeply into the mechanism for the salt concentration dependence with PFG SE NMR and MD simulations.[3] It can be clearly seen from the trend of **P-PI**, **P-PI/LiOTf0.4**, and **P-PI/LiOTf1**, that the segmental motion of the PDMS chains slow down when forming complexes with LiOTf, and decrease further at higher LiOTf concentration (Figure 2.11a), because the formation of metal-ligand coordination adds temporary constraints to the chain ends.[53] The diffusion of OTf^- also slows down at higher LiOTf concentration, confirming that the anion motion is associated with the chain motion. Interest-

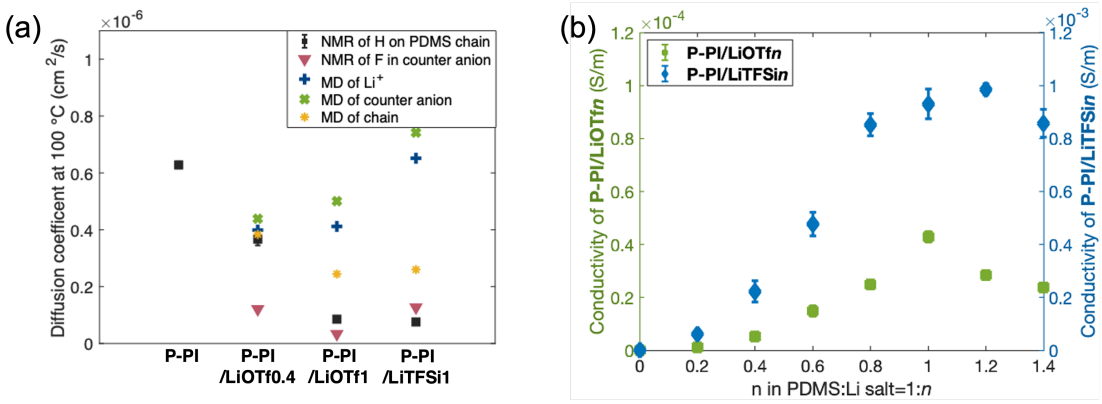

Figure 2.11: Li^+ coordinated PDMS. (a) A comparison of diffusion coefficients from both experimental and simulation results: diffusion coefficients of ^1H from PDMS chain and ^{19}F from counter anions in Li salts are obtained from PFG SE NMR measurements at 100 °C, and diffusion coefficients of Li^+ and counter anions are obtained from MD simulation at 100 °C. Error bars are calculated from ^1H in different moieties on the PDMS chain; (b) Ionic conductivity of LiOTf and LiTFSi coordinated PDMS with varying salt concentration.[3]

ingly, while the MD calculated diffusion at 100 °C also shows decreased chain mobility at increased LiOTf concentration, it actually shows a slight increase in ion diffusivity. The MD result would suggest that the thermally enhanced clustering[102, 103] is more important than reduced chain mobility at increased concentration, in contrast to the experimental result.

2.2.4 The effect of cation identity

We next study the effect of coordination strength on the ionic conductivity of the metal-ligand coordinated PDMS by using a multivalent cation, Cu^{2+}. To obtain the coordination structure, a small-molecule Cu^{2+}-pyrdiyl imine complex is synthesized by adding copper trifluoromethanesulfonate ($Cu(OTf)_2$) into the

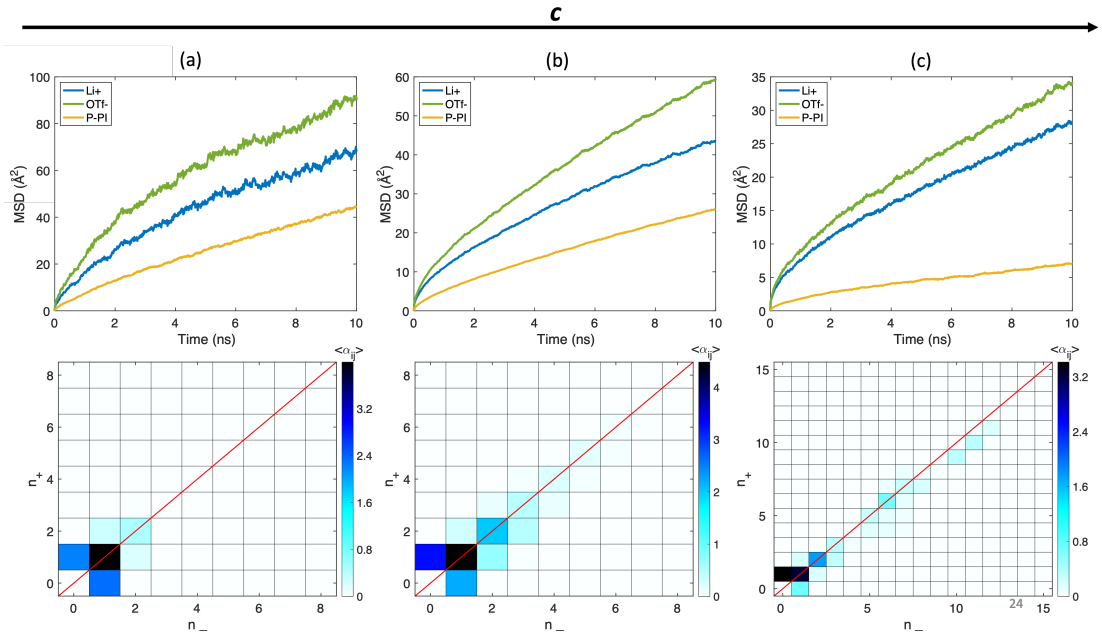

Figure 2.12: MSD plot of mobile species and cluster analysis for (a) **P-PI/LiOTf0.4**; (b) **P-PI/LiOTf1**; (c) **P-PI/LiOTf2.0**.

model ligand N-propyl(2-pyridyl)methanimine. The mass spectrum shows that the ratio between Cu^{2+} and pyridyl imine ligand is 1 : 2 (Figure 2.13a).[54, 104] We expect that Cu^{2+} forms a stronger and more stable complex than Li^{+}, yielding a less dynamic network, which can be characterized by the rheology of the PDMS complexes. We first compare the coordination strength of Li^{+} and Cu^{2+} by examining the rheological curves of **P-PI/LiOTf1** and **P-PI/Cu(OTf)$_2$1**: the storage and loss moduli (G' and G'', respectively) of **P-PI/Cu(OTf)$_2$1** are orders of magnitude higher than the moduli of **P-PI/LiOTf1** within the full frequency range measured. In **P-PI/Cu(OTf)$_2$1**, $G' > G''$ and G' remains independent of the frequency, indicating that the material is in the rubbery plateau region due to the presence of strong metal-ligand coordination, which act as transient crosslinks in the polymer; whereas in **P-PI/LiOTf1**, $G' < G''$, indicating that the material is in the terminal region, where chains relax quickly and the material behaves like

a viscoelastic fluid.[3, 105] The difference in viscoelasticity of the Li^+ and Cu^{2+} coordinated PDMS can also be directly seen from the photos of **P-PI/LiOTf1** and **P-PI/Cu(OTf)$_2$1** samples: the former is a viscous liquid and the latter is a flexible film, confirming that Cu^{2+} yields much stronger bonding with the ligand functionalized PDMS than Li^+ (Figure 2.13b).

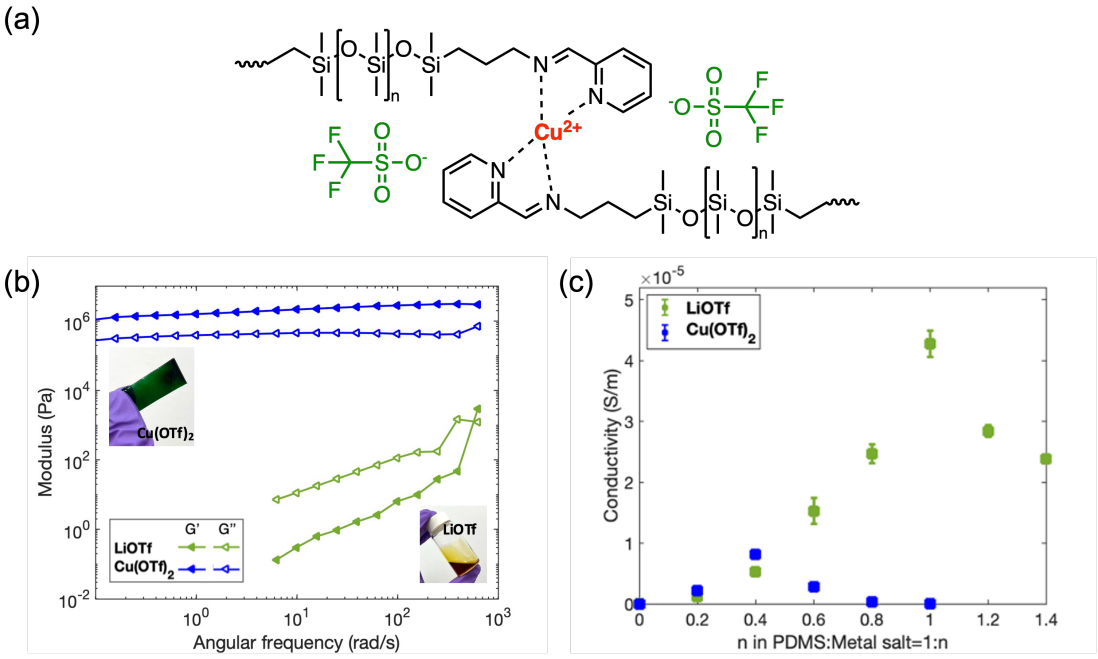

Figure 2.13: Cu^{2+} coordinated PDMS. (a) The chemical structure of **P-PI/Cu(OTf)$_2$1** predicted from the mass spectrum; (b) Frequency sweeps at a strain of 0.1% measured by rheology, with sample photos of **P-PI/Cu(OTf)$_2$1** and **P-PI/LiOTf1**;[3] (c) The variation of ionic conductivity of the polymer.[3]

To study how the coupled Cu^{2+} ion concentration and network dynamics together affect the ionic conductivity of the material, we measure the ionic conductivity of the PDMS complex as a function of $Cu(OTf)_2$ concentration, showing quite a different trend than in the Li^+ coordinated system (Figure 2.13c). We note that the $Cu(OTf)_2$ coordinated PDMS, regardless of salt concentration, cannot achieve nearly as high conductivity as the maximum value

of the LiOTf coordinated PDMS. The maximum ionic conductivity is obtained at **P-PI/Cu(OTf)$_2$0.4**, which is far lower than the maximum coordination capacity. In addition, a drastic decrease of the ionic conductivity is observed beyond this peak. Increasing Cu(OTf)$_2$ concentration from **P-PI/Cu(OTf)$_2$0.2** to **P-PI/Cu(OTf)$_2$0.4** improves the ion concentration and therefore increases the ionic conductivity of the material. However, the trend is interrupted by the slowing of polymer dynamics in the system at higher Cu(OTf)$_2$ concentration. For **P-PI/Cu(OTf)$_2$0.6**, **P-PI/Cu(OTf)$_2$0.8**, and **P-PI/Cu(OTf)$_2$1**, the ion motion slows down due to the significantly extended chain relaxation.[3] Another interesting observation is that the Cu^{2+} system is more ionically conductive than the Li^+ system at the low salt concentration of PDMS:salt=1 : 0.2 and 1 : 0.4 (Figure 2.13c). This can be attributed to the valency of the metal cation: Cu^{2+} is balanced by two OTf^- anions whereas Li^+ only has one, so when adding the same number of moles of LiOTf and Cu(OTf)$_2$ salt into the PDMS, the ion concentration is higher in the Cu^{2+} system than the Li^+ system, which promotes the high ionic conductivity.

The MD simulation results in Figure 2.14(a), (b) and (d) shows that the most probable coordination number for copper is 6, with the nitrogen atoms on the ligands. The calculated NE conductivity for **P-PI/Cu(OTf)$_2$1** is 0.011 S/m (extrapolated from Figure 2.14(c)). We can observe that, the MSD curve of Cu^{2+} highly overlap with that of the polymer chains indicates that the coordination between is strong and less dynamic. In addition, the diffusion coefficents or more intuitively, the magnitude of MSD, indicates that the motion of mobile species is nearly freezing, which can be due to decreased free volume or increased T_g. The viscosity of **P-PI/Cu(OTf)$_2$1** using NEMD simulation is 98 cst at a shear strain rate of $10^9/s$, while the viscosity of **P-PI/LiOTf1** is 16 cst at the

same strain rate. The commercial pristine PDMS for experimental use is about 20 *cst*.

The deviation between the simulated and experimental conductivity can be that 1) we fail to capture the effect of slowing down ion motion due to the greatly reduced free volume caused by phase change from MD simulations. It is confirmed experimentally by a much higher T_g and apparent activation energy compared to the Li^+ counterpart; 2) The coupled force field functional form might not be accurate enough to represent the complex structure or describe the strength of the metal-ligand coordination.

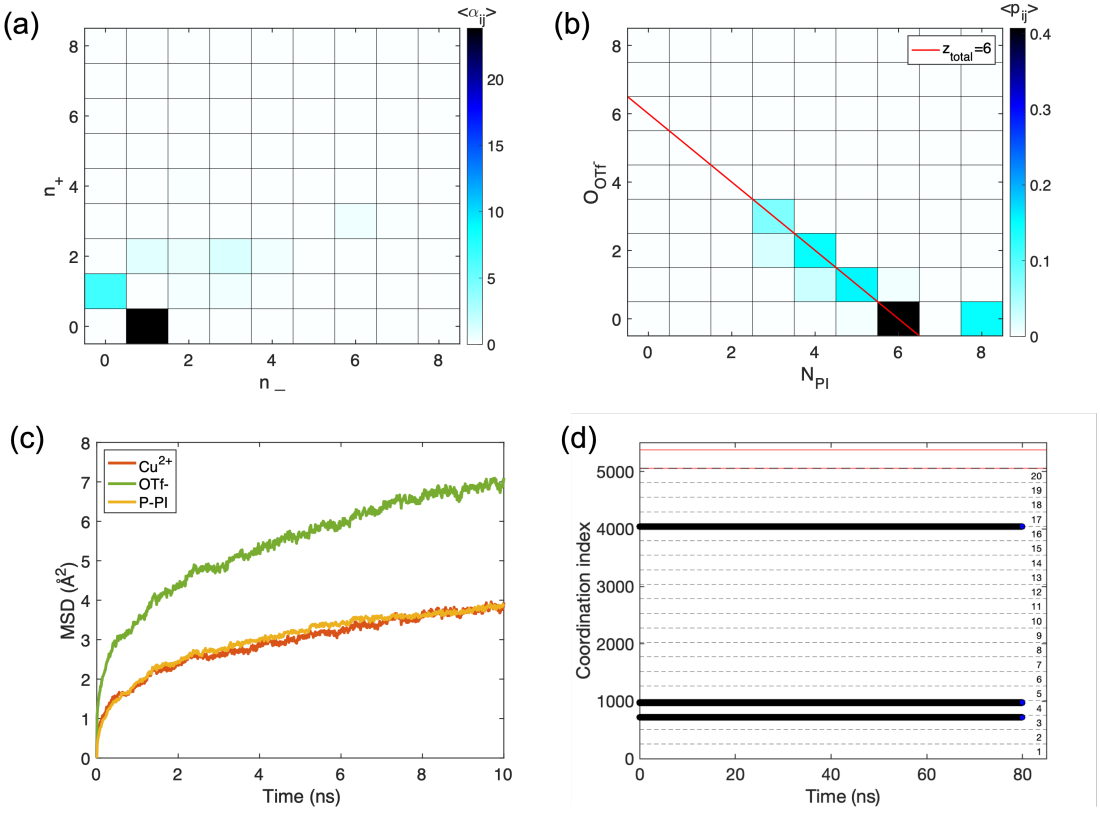

Figure 2.14: MD simulation results for **P-PI/Cu(OTf)$_2$1**. (a) Ion clustering statistics; (b) coordination matrix; (c) MSD plots of mobile species; (d) variation over time of atom indices coordinating a specific copper ion.

CHAPTER 3

POLYELECTROLYTE DIODE

Considerable research effort has led to significant advancements in the realm of electronics based on conductive polymers,[106–108] which have been widely employed to create organic p-n junctions in solid-state devices, akin to the p-n junctions found in traditional silicon-based electronics.[4, 109–112] There are three types of diodes, based on the chemical identity of the mobile carriers in each polymer as well as the mode of transport dominant in each polymer.[16] Type I diode has annihilating ions with significant Donnan exclusion, which is commonly created with bipolar membranes placed between aqueous acid and base solutions. The membranes typically have high density of fixed charges and are selective to H^+ and OH^-. Under forward bias, H^+ and OH^- migrate toward the junction and combine to form water, which then diffuses away from the junction (similar to electron/hole annihilation in a traditional semiconductor PN junction). Under reverse bias, the mobile ions migrate away from the junction, leaving a region without charge carriers. This creates a large electric field that opposes the applied voltage and thus very little current flows in the device. If the reverse bias junction electric field is large enough, and there is a neutral species present in the junction made from the mobile ions (like H_2O), then this field can rip that neutral species apart into separate mobile charges and current will flow. This reverse bias breakdown can be intentionally used or suppressed.[16] Compared to Type I diode, type II diode has annihilating ions but without significant Donnan exclusion. These diodes can be made from a hydrogel polyelectrolyte or a neutral gel, which does not exclude neutral salts. The rectification direction depends on the relative concentration of ionic charge carriers in baths bordering either side of the gel. Under forward bias, migration of

the non-annihilating counterions dominates. Under reverse bias, the current is lower because chemical recombination of the annihilating ions creates a region of neutral species right at the bath/polymer junction that is higher in resistance than the bulk polymer. If the gel is neutral, this device is called an electrolytic diode.[16]

This work focuses on type III diodes which describe junctions between most polyelectrolytes and have non-annihilating ions with Donnan exclusion. Under forward bias, the concentration of mobile carriers increases until it is sufficient to drive minority carriers into the opposing region. Therefore, forward bias current must be carried by minority carriers. Reverse operation is similar to type I, but if non-hydrogel polyelectrolytes are used, can sustain larger reverse voltages without breakdown. Recently, type III diodes have been constructed from aqueous polyelectrolytes. One popular choice is to use poly(sodium 4-styrenesulfonate) (PSS) and poly(diallyl dimethylammonium chloride) (PDADMA) as the polyanion and polycation respectively, with platinum foil as the electrode.[4, 113, 114] Carye et al. and Zhang et al. used these polymers directly while Wang et al. embedded them in a double network. The direct use of the polymers led to a much higher rectification ratio, but limited the device stretchability, while the double network diode retained performance up to a stretch of 4. One disadvantage of these water based systems was that the breakdown voltages were low. At around -2 V, the currents began to increase dramatically as water was dissociated at the junction. Because the electrodes in these devices were made from platinum or silver and thus semipolarizable, the measured response of the diode was a function of the electrode interface in addition to the polyelectrolyte junction. For example, while the open circuit voltage of the system was likely in the hundreds of mV range [114], the device only

conducted well in forward bias above 2 V when the platinum electrodes were able to split water efficiently[115]. Han et al made a similar type III diode with nonpolarizable electrodes and demonstrated a turn on voltage near 0 V.[111]

There have been limited attempts to tackle polyelectrolyte (gel) diodes through molecular level simulations.[116–118] Triandafilidi et al. and Li et al. both setup the simulation box assuming a cubic lattice of cross-linking nodes. The idealization of the chain configuration presents a simplified model polyelectrolyte gel diode formed by a junction of two oppositely charged crosslinked polyelectrolyte networks. However,the typical polyelectrolytes, PSS and PDADMA, commonly used for experimental and computational study of polyelectrolyte complexes and multilayers, are linearly polymerized. This work investigates into the coarse-grained MD simulations of polyelectrolyte diodes formed by a junction of PSS and PDADMA. Four main metrics, rectification ratio, forward bias current, (reverse) breakdown voltage and switching time, are captured to evaluate the performance of an ionic diode from a nanoscale perspective.

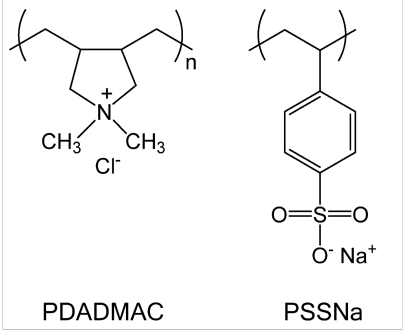

Figure 3.1: The chemical structure of PDADMA and PSS

3.1 Methods

3.1.1 Simulation details

The coarse-grained MD simulations are performed using the GROMACS-2022.5 software package.[119–121] Initial configurations are generated with the Polyply python suite.[122] All interaction parameters are from the MARTINI force field.[123–125] The simulation box contains either 30 chains of PSS or 30 chains of PDADMA with a degree of polymerization $N_m = 30$. Periodic boundary conditions are applied in three orthogonal directions. The temperature in all equilibrium production runs is $T = 298K$. The number of ions and polarizable MARTINI water beads is 900 and 250, respectively. For the dry polymer case (i.e. without water), the initial configuration is created by inserting all components randomly into a cubic simulation box of side length ($b_x = b_y = b_z = 7\ nm$). The above systems are then equilibrated with a standard protocol of energy minimization, followed by a 2 ns of NVT and 2 ns of NσT simulation, with a time step of 20 fs. NσT is essentially an NPT ensemble but with semi-isotropic pressure coupling. This means that the dimensional fluctuations in x and y will be equal in proportion and independent from those in z, which preserves the aspect ratio of the x-y plane. For the semi-isotropic coupling, a Berendsen thermostat with the characteristic time $\tau = 1\ ps$ and a Berendsen barostat at a pressure of $p = 1\ bar$ with the relaxation time $\tau = 3\ ps$ and the compressibility 3×10^5 bar^{-1} are used. In order to save computation time, only cutoff electrostatic interactions are used in the equilibrium procedure. The relative dielectric constant of the medium is set 2.5 to represent the implicit existence of the polymer scaffold.

After equilibrating each system, we use VMD to bring the two individual

slabs into contact and modify the box size in z dimension. With $b_z = 50\ nm$, the box is made pesudo-periodic with two free surfaces in z direction. The assembled system is equilibrated again with energy minimization and NVT ensemble for 5 ns. The production run is performed for 200 ns with a time step of 20 fs in the NVT ensemble at a temperature of $T = 298\ K$. For all simulations, a V-rescale thermostat with the characteristic time $\tau = 1\ ps$ are used. The neighbor lists have a range of 1.2 nm and updates are performed each 5 time steps. The cutoff radius for Lennard-Jones interactions is 1.2 nm and the interactions are shifted to zero beyond 0.9 nm. The PME direct space cutoff radius was 1.2 nm and the spacing of the Fourier grid was 0.12 nm. A static field with $E_0 = -0.1\ V/nm$ is applied in the z direction.

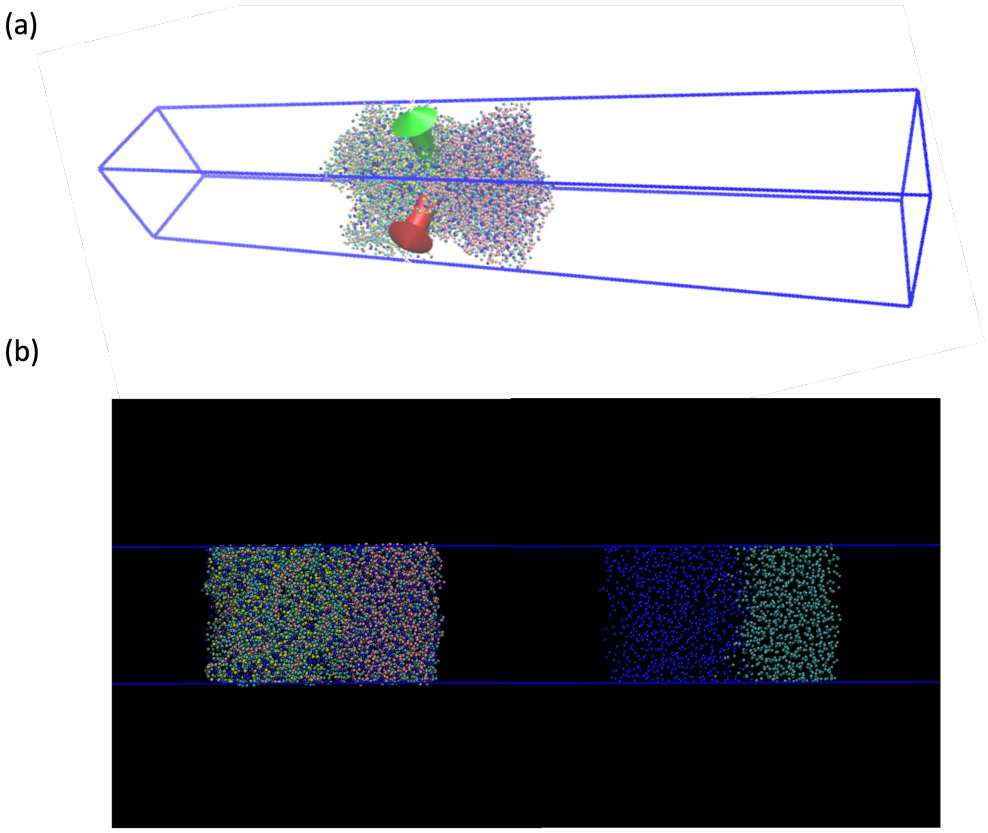

Figure 3.2: (a) The setup of the diode simulation; (b) The schematic of the whole system (left) and ions only (right) after forward bias.

3.1.2 Static ionic conductivity

An electrical current **j** can be observed if an electric field E_0 is applied to a conducting system, where E_0 stands for the Maxwell field. The empirical finding Ohm's law demonstrates the relation between the current and a given field:

$$\mathbf{j} = \sigma \times E_0 \tag{3.1}$$

where σ is the conductivity of the system. It is necessary for experiments to apply an electrical field to measure the conductivity which leads to non-equilibrium conditions. However, it is inconvenient to introduce external field into Newtonian equations of motions, e.g.

$$m_i \frac{d^2 r_i}{dt^2} = \nabla U(r_1, ...r_N) + \sum_{i=1}^{N} q_i \mathbf{E}(t) \qquad i = 1, ..., N \ for\ a\ N particle\ system \tag{3.2}$$

where m_i, r_i and q_i is the mass, position and charge of i^{th} particle. It would either lead to a rise in temperature, a drift in energy and center-of-mass, or provoke currents outside the linear response regime [126] if the field was too strong, or be swamped by noise if it was too weak. However, the Fluctuation-Dissipation theorem states that small fluctuations, in other words the noise, of dynamical variables in equilibrium systems behave, or literally relax, in just the same way as the dynamic variable in a non-equilibrium system induced by an external field would.[127] R. Kubo also brought about the mathematical explanation and proof for the conjugate fluxes to mechanical field.[128] The Green-Kubo formula for conductivity is:

$$\mathbf{j} = \frac{\Delta \mathbf{J}(\omega)}{V} = \frac{1}{V k_B T} \left(\int_0^\infty e^{i\omega t} \langle J(t) J(0) \rangle \ dt \right) \mathbf{E}(\omega) \tag{3.3}$$

where

$$\sigma(\omega) = \frac{1}{V k_B T} \int_0^\infty e^{i\omega t} \langle J(t) J(0) \rangle \ dt \tag{3.4}$$

From eq 3.3 and 3.4, it is possible to simulate non-equilibrium systems, record the occurring fluctuations in dynamical variables, in this case the current, and calculate non-equilibrium properties, the conductivity. The Einstein-Kubo-Helfand (EH) formula demonstrates an analogous relation between the mean square displacement of the translational dipole moment, the integral of the current

$$M_J = \int_0^\infty \mathbf{J} dt \tag{3.5}$$

and the conductivity

$$\sigma(\omega = 0) = \frac{1}{3Vk_BT} \int_0^\infty \langle J(t)J(0)\rangle \; dt \tag{3.6}$$

$$= \frac{1}{6Vk_BT} \lim_{t\to\infty} \frac{\left\langle \Delta M_J(t)^2 \right\rangle}{t} \tag{3.7}$$

In other words, the static conductivity can be obtained from the linear slope of the mean-squared displacement of the translational dipole moment. The dielectric constant as determined experimental can be represented by

$$\epsilon_{stat} = \frac{4\pi}{3Vk_BT} \cdot \left\langle M_{tot}(t)^2 \right\rangle + 1 \tag{3.8}$$

$$= \frac{4\pi}{3Vk_BT} [\left\langle M_D(t)^2 \right\rangle + 2\langle M_D(t) \cdot M_J(t)\rangle + \left\langle M_J(t)^2 \right\rangle] + 1 \tag{3.9}$$

which is composed of rotational M_D and translational M_J components. In addition to the respective self-terms, the cross term standing for translational-rotational coupling is included, too. Since M_D is measured to be zero,

$$\epsilon_{stat} = \frac{4\pi}{3Vk_BT} \cdot \left\langle M_J(t)^2 \right\rangle + 1 \tag{3.10}$$

and the Debye length of the ionic double layer or the ionic junction can be estimated using

$$\lambda_D = \left(\frac{\epsilon_r \epsilon_0 k_B T}{\sum_{i=0} \rho_{\infty i} e^2 {z_i}^2}\right)^{1/2} \tag{3.11}$$

where ϵ_r is the dielectric constant of the system, ϵ_0 is the permittivity of free space, $\rho_{\infty i}$ is the number density of ion type i, e is the elementary charge and z_i is the ion valency.

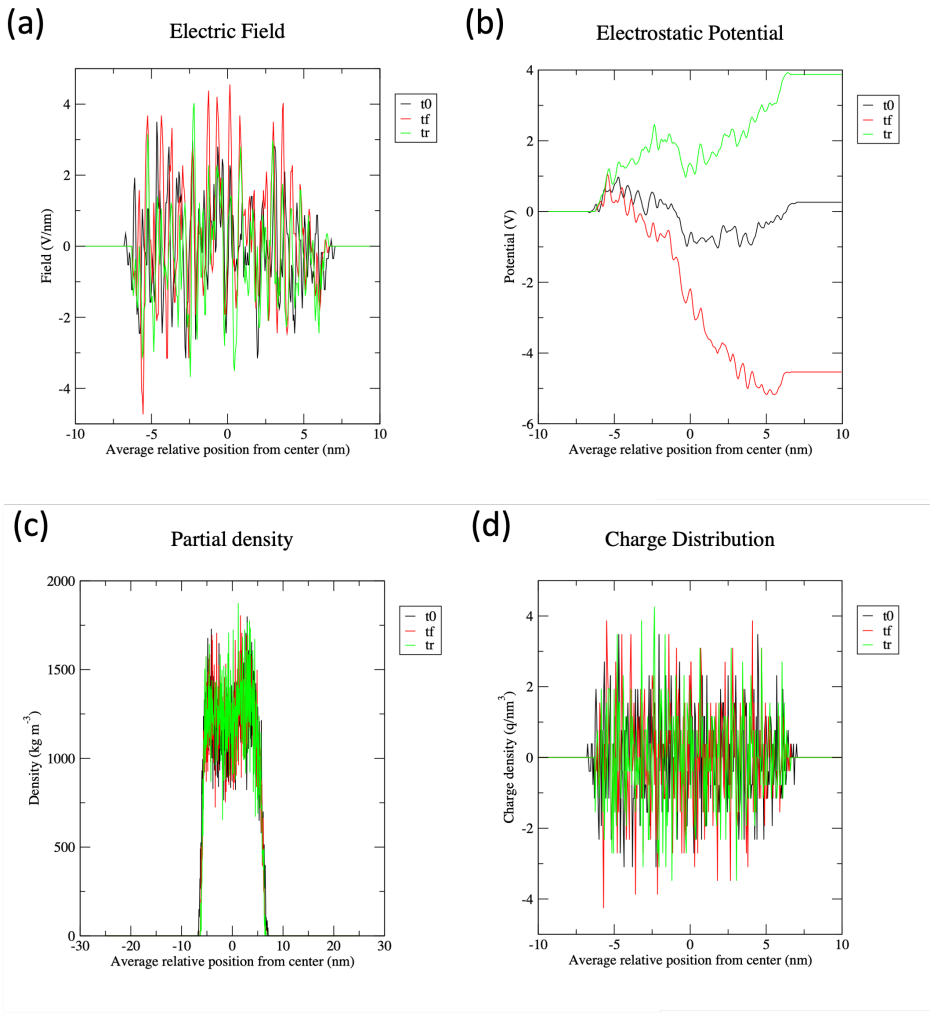

Figure 3.3: (a) Electric field; (b) electrostatic potential; (c) partial density; (d) charge distribution with respect to the average relative position from center across the lateral dimension (z) of the box. t_0 is at equilibrium, t_f is after forward bias and t_r is after reverse bias.

3.2 Results and Discussion

3.2.1 Dry polymer

We start our investigation by demonstrating the dry polymer case without water molecules involved. From Figure 3.3, we show the spatial charge density profiles and electrostatic potential at equilibrium, forward bias and reverse bias under an electric strength of 0.1 V/nm. It is observant that the density distribution and potential drop is more prominent near the junction, which indicates the existence of the ionic double layer caused by the interpenetration or entanglement between the oppositely charged polyelectrolytes. The blue and red curve in Figure 3.4(a) represent the forward bias after equilibrium and the reverse bias following the forward bias respectively, the difference between which indicates that the rectification effect is well captured by the MD simulation (J_f/J_r = 7). The inset from Cayre et al. shows good consistency that the experimental rectification ratio of PSS-PDADMA diode is about 8 after reaching steady state. The green and blue curve in Figure 3.4(a) represent the forward bias after 200 ns reverse bias and the reverse bias following the forward bias. The purpose of applying reverse bias at first is to deplete possible mobile ions existing within the junctions. It is found that while the current density and ionic conductivity is about one magnitude lower than that of the simulation starting from equilibrium, the rectification ratio is much higher (J_f/J_r = 25). The dielectric constant measured using EH method is of magnitude 10^1. With the dielectric constant obtained, the Debye length is estimated to be 0.2 nm and the thickness of the ionic double layer is 0.4 nm. Furthermore, we sweep the simulation over the strength of electric field under forward bias, as shown in Figure 3.4(b). Increas-

ing the electric field enhances the mobility of ions through the polymeric matrix therefore gives better forward current density. One interesting phenomenon is that the mobility of ions dramatically decreases under the strength of 1 V/nm, which indicates possible breakdown or longer simulation time required to behave after depletion.

3.2.2 Polyelectrolyte gel

We next investigate into the wet polymer diode case with 2%wt molecules for each slab under an electric field of 0.02 V/nm. Water electrolysis is not considered for the sake of simplification. In fact, excluded bonds within water molecules would be over-rotated or over-stretched with a bias exceeding 0.05 V/nm. With the existence of water molecules, the transport of ions can be facilitated a lot. Figure 3.5 indicates that the wet diode has much higher current density compared to the dry diode for both forward ($J_{f,wet}/J_{f,dry}$ = 26) and reverse bias ($J_{r,wet}/J_{r,dry}$ = 23). However, the rectification ratio for the wet diode ($J_{f,wet}/J_{r,wet}$ = 1.5) is just higher than that for the dry diode ($J_{f,wet}/J_{r,wet}$ = 1.3). Here, we propose some guesses about the potential restrictions of the MD simulations that might cause deviation from the physical truth: 1) since no water electrolysis is assumed nor allowed, there are no hydroxide and hydrogen ions entering the membrane where they are supposed to combine to form water and dramatically decrease the local conductivity in the backward direction; 2) since we are using the polarizable water models, the water molecules can have certain dipole moment and form water clusters under different bias assuming no electrolysis, which can affect the ion transport; 3) We speculate that with 2% water content, the water clusters existing can be fragmented into small and discon-

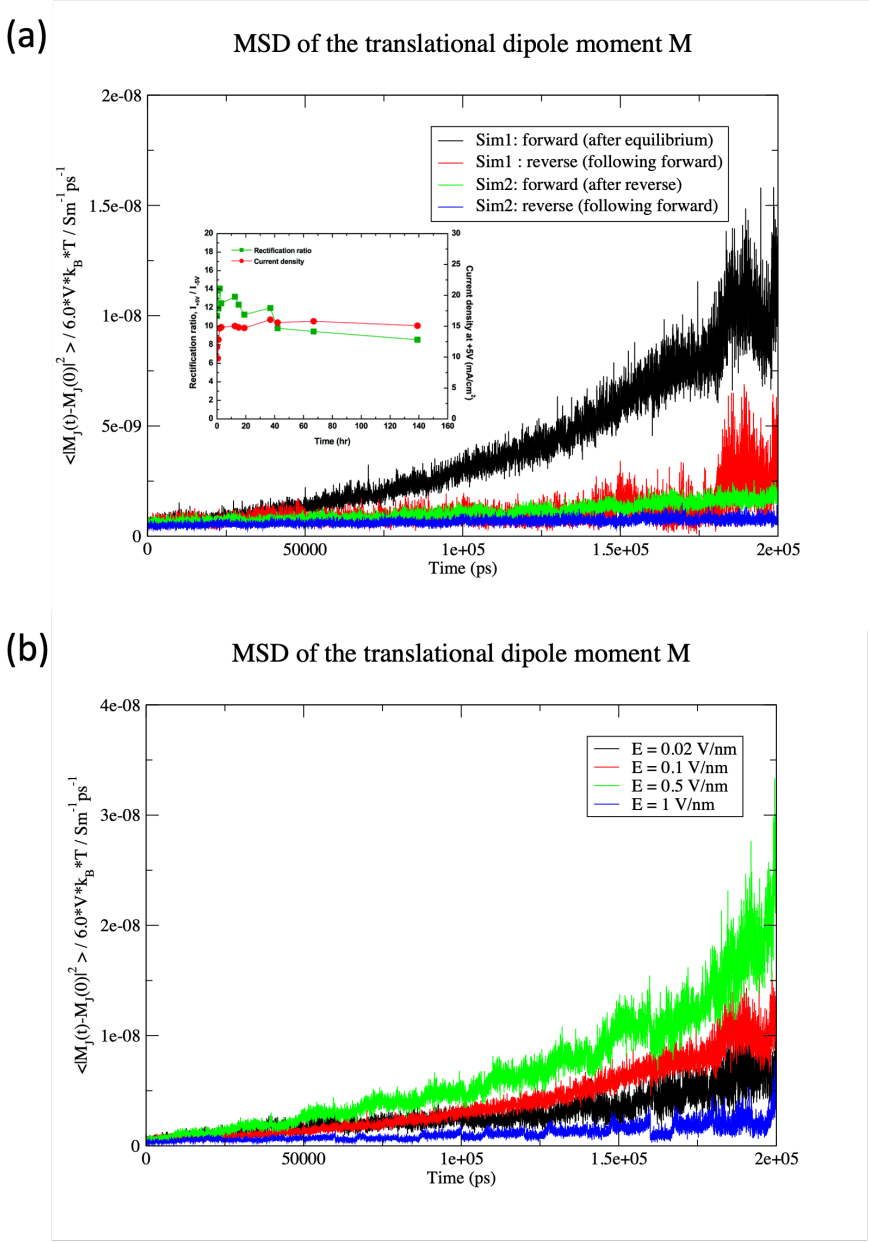

Figure 3.4: MSD of the translation dipole moment versus time for (a) simulations under different initial conditions. Sim1 demonstrates that the forward bias directly start after equilibrium and Sim2 demonstrates that the forward bias follows an initial reverse bias. Inset copied from Cayre et al[4]. (b) forward bias under different electric field strengths.

nected, however, with higher water content, the water clusters can grow and coalesce into percolative water channels or paths where ions can move freely,

and therefore cause a different behavior in rectification effect.[20] This represents an interesting subject for further computational studies.

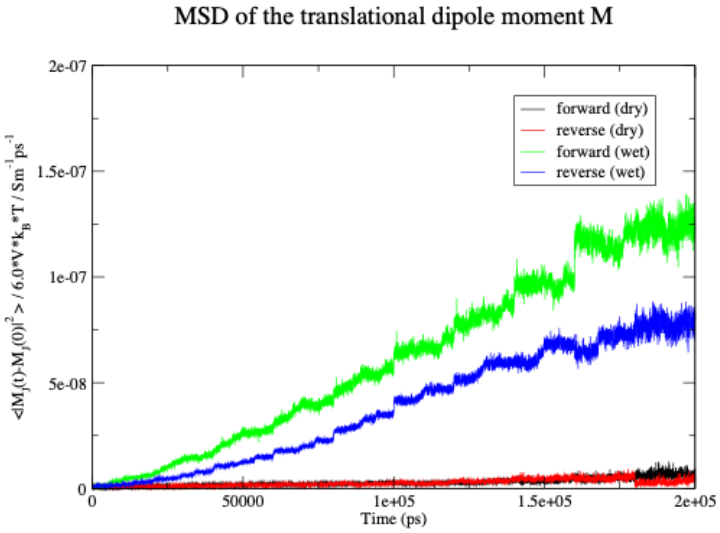

Figure 3.5: MSD of the translation dipole moment versus time for dry and wet diodes under forward and reverse bias at 0.02 V/nm

Furthermore, we run a convergence study to determine the steady state or the switching time, which refers to how long the diode takes to reach a steady state current after a transition from reverse to forward bias or vice versa. We assume that the convergence is achieved with less than 20% drop. Figure 3.6 shows that the conductivity of the dry diode reaches convergence at 2000 ns while the wet diode converges faster at 1000 ns. The contrast between the switching time of the dry and wet diode indicates that water plays the role in fast ion transport and polymer dynamics therefore establishing sooner steady state.

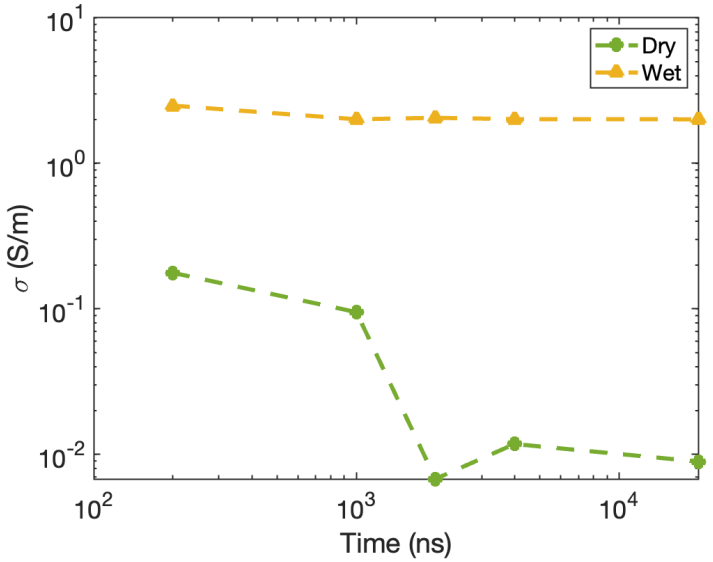

Figure 3.6: The steady state or switching time analysis for diodes. σ is the ionic conductivity under forward bias, where dry diode is at 0.1 V/nm and wet diode is at 0.02 V/nm.

CHAPTER 4

CONCLUSIONS AND FUTURE DIRECTIONS

For the first part of this work, we investigate the ion conductivity mechanism of a metal-ligand coordinated polymer whose model system is consisted of pyridyl imine functionalized PDMS and two metal cations Li^+ and Cu^{2+}. We first confirm that the formation of metal-ligand complex promotes ion dissociation in the polymer matrix by showing increased ionic conductivity of the ligand-functionalized PDMS compared to the pristine PDMS. MD simulations prove that cation-anion dissociation is facilitated by the interaction of metal cations and ligands attached to the polymer. Based on this finding, a series of Li^+ coordinated PDMS with different counter anions of the salt are synthesized to investigate the effect of cation-anion interactions on the ionic conductivity of the polymer. We find that a bulkier anion not only yields stronger Li^+-ligand coordination but also suppresses the tendency for ion precipitation, promoting higher ionic conductivity. In addition, MD simulations show that bulkier anions with higher delocalized charge tend to have more frequent intercluster hopping and form more negatively charged clusters. The effect of salt concentration is next studied, which is seen to enhance the ionic conductivity of the complex by increasing the ion concentration up to a point. However, for the Li^+ cation systems, the ionic conductivity reaches the maximum when the ligand coordination capacity is saturated, and then starts to decrease at the higher salt concentrations since the additional salt preferentially forms clusters. MD simulations confirm that the chain segmental motion is also hindered by increasing salt loading, though this seemed to be of secondary influence for the Li^+ system. To investigate the effect of coordination strength on the ionic conductivity of the polymer, we study on Cu^{2+} coordinated PDMS. We show that as expected from

the experimental rheological measurements, Cu^{2+} forms a much stronger coordination with the ligand on the PDMS than Li^{+}. The higher viscosity measured from the Cu^{2+} coordinated PDMS system indicates a rapid decrease of polymer dynamics. This work explores the structure-property relationship of the metal-ligand coordinated PDMS as a novel polymer electrolyte. At a superficial level the governing mechanisms are similar to other polymer electrolytes – salt solvation, chain mobility, ion clustering, ion diffusion, and ion hopping – however, their relative importance and how they are controlled by the polymer structure and salt selection are quite distinct. These insights will enable more strategic future material design of low T_g ionically conductive polymers. For future work, polarizable force field could be considered to describe the metal-ligand coordination strength more accurately.

For the second part of this thesis, we investigate into the ion transport mechanism and performance of polyelectrolyte diodes formed by a junction of PSS and PDADMA. We first confirm the existence of the ionic double layer caused by the interpenetration or entanglement at the junction for dry polymer case. MD simulations well capture the rectification effect under forward bias and reverse bias. A pre-depletion procedure with reverse bias can be helpful for an enhanced rectification effect while decreasing the current density. To investigate the role of water in ion transport, we further study the wet polymer case with 2% water content. Our MD simulation results show that the wet diode has higher current density than the dry diode but basically the same rectification effect, which could be due to the assumption of no water electrolysis. There are still a lot of other factors or perspectives one can explore into this project, e.g. how the fragmentation from percolative water path or pore networks into small and disconnected clusters affect the ion transport as water content de-

creases, how the molecular weight or the polymer concentration affect the ion transport, how the mechanical harvesting property of the diode is, or what is polymer dynamics happening exactly at the junction. For further work, ReaxFF or other ab-initio MD should be considered for further research when coming to the electrode reaction or water electrolysis, which are important factors in ionic devices. Machine-learning interatomic potentials can be used to probe into ion diffusion or ion/water clustering event and simultaneously keeps the accuracy at the density functional theory level.

Previous effort on diode methods in bullet points (for lab folks who are going to continue this project):

1. I tried using non-periodic boundary conditions (only periodic in xy). Note using non-periodic boundary conditions will have to add walls. I added 12-6 walls consisted of carbon atoms but the left wall and right wall failed to exert equal forces on the system. This should not happen on perfectly equilibrated system. Future effort could be devoted to solve the wall problem since building up with the non-periodic boundary conditions with walls should be the most convincing and realistic approach. And it will be also convenient to add electrodes as walls.

2. after failing with the first setup, I turned to the pseudo-periodic conditions, the method described in the main text of my thesis. In simple words, we increase the box dimension in z direction. But the problem with this method is that we are still not clear about the effect of the free surfaces in the lateral direction on the system. And ions were escaping the box when applying a higher

reverse bias even forward bias, which caused a failure. This can be solved if you solve 1.

3. I also tried complete periodic boundary conditions for the system with longer lateral dimension so that the bulk material in each slab can serve as a reservoir. In this way, the image next to each other should not affect the performance of ionic junctions. But after equilibrating each slab like before and putting them together and minimizing energy, Gromacs returned error of "the distance between excluded atoms exceeds the cutoff distance". I visualized the molecules, they are whole and not broken across the boundaries. And someone in Gromacs forum said that updating to Gromacs2023.2 solved this for no reason. I am using Gromacs2022.5, since the g2 cluster are using a lower version of cmake which cannot compile gromacs2023.2, but I did try running simulation using Gromacs2023.2 on my local workstation and it worked.

APPENDIX A

APPENDIX 1

```
# LAMMPS input script for standardized atomistic simulations
# Created by emc_setup.pl v4.1, August 1, 2021 as part of EMC
# on Wed Apr 27 13:21:26 EDT 2022

# LAMMPS atomistic input script

echo            screen
units           real
atom_style      full
boundary p p p

# Variable definitions

variable        project         index   "polymer"       # project name
variable        source          index   .       # data directory
variable        params          index   .       # parameter directory
variable        temperature     index   303             # system temperature
variable        tdamp           index   50              # temperature damping
variable        pdamp           index   500       # pressure damping
variable        dielectric      index   1.0             # medium dielectric
variable        kappa           index   4               # electrostatics kappa
variable        cutoff          index   12.0            # standard cutoff
variable        charge_cutoff   index   12.0            # charge cutoff
variable        precision       index   0.00001                 # kspace precision
variable        lseed           index   723853                  # langevin seed
variable        vseed           index   981020                  # velocity seed
variable        tequil          index   10000000        # equilibration time
variable        dlimit          index   0.1             # nve/limit distance
variable        trun            index   80000000                # run time
variable        frestart        index   1               # 0: equil, 1: restart
variable        dtrestart       index   20000           # delta restart time
variable        dtdump          index   20000           # delta dump time
variable        dtthermo        index   20000           # delta thermo time
variable        timestep        index   0.5             # integration time step
variable        tfreq           index   50              # profile sampling freq
variable        nsample         index   400             # profile conf sampling
variable        dtime           equal   ${tfreq}*${nsample}   # profile dtime
variable        restart         index   ${params}/${project}.restart2

if "${frestart} != 0" then &
"variable       data            index   ${restart}" &
else &
"variable       data            index   ${params}/${project}.data" &
```

```
# Interaction potential definition

pair_style lj/class2/coul/cut ${cutoff} ${charge_cutoff}
bond_style      class2
angle_style     class2
dihedral_style class2
improper_style          class2
pair_modify     mix sixthpower tail yes
special_bonds lj/coul 0 0 1

if "${frestart} != 0" then "read_restart ${data}" else "read_data ${data}"
include         ${params}/${project}.params

neighbor 2.0 bin
neigh_modify  delay 0 every 1 check yes

# Integration conditions (check)
timestep        ${timestep}
dielectric      ${dielectric}
fix             mom all momentum 100 linear 1 1 1 angular

group liion type 1
group otfion molecule 21:40
group backbone molecule 1:20
group ion union liion otfion
group mcoord type 1 7 8 9

if "${frestart} != 0" then "jump SELF simulate"

# Minimization
#fix min all box/relax aniso 0.0 vmax 0.001
min_style sd 1e-5
minimize 1e-25 1e-25 5000 10000

min_style cg 1e-5
minimize 1e-25 1e-25 5000 10000
#unfix min

# specify initial velocity of atoms
velocity        all create ${temperature} ${vseed} &
                dist gaussian rot yes mom yes sum yes
#run 0
#velocity       all scale ${temperature} dist gaussian rot yes mom yes sum yes
```

```
reset_timestep 0
thermo          ${dtthermo}
thermo_style custom step temp pe etotal lx ly lz vol density press pxx pyy pzz
dump        1 all custom 5000 equilibration.lammpstrj id type x y z

# constant room temp
fix nvt_eq all nvt temp ${temperature} ${temperature} ${tdamp}
restart     ${dtrestart} ${project}.restarteq1 ${project}.restarteq2
run 5000000
unfix nvt_eq

#room temp and pressure
fix npt2 all npt temp ${temperature} ${temperature} ${tdamp} aniso 1.0 1.0 ${pdamp} drag 0.2
restart     ${dtrestart} ${project}.restarteq1 ${project}.restarteq2
run 5000000
unfix npt2

undump 1
write_restart   ${project}.restarteq

# Simulation

label           simulate

# Integrator
#reset_timestep 0
thermo          ${dtthermo}
thermo_style custom step temp pe etotal lx ly lz vol density press pxx pyy pzz

pair_style lj/class2/coul/long ${cutoff} ${charge_cutoff}
bond_style      class2
angle_style     class2
dihedral_style class2
improper_style      class2
pair_modify     mix sixthpower tail yes
special_bonds lj/coul 0 0 1

include         ${params}/${project}.params
kspace_style pppm/cg ${precision}

#fix            temp all langevin ${temperature} ${temperature} ${tdamp} &
#               ${lseed}
#fix            int all nve
```

```
fix           nvt3 all nvt temp ${temperature} ${temperature} ${tdamp}
#fix          3 all efield 5e-8 0.0 0.0
#fix_modify 3 energy yes
#fix_modify 3 virial yes


# System sampling: pressure
#fix                sample_press all ave/time ${tfreq} ${nsample} ${dtime} &
#                   c_thermo_temp &
#                   c_thermo_press[1] c_thermo_press[2] c_thermo_press[3] &
#                   c_thermo_press[4] c_thermo_press[5] c_thermo_press[6] &
#                   file ${project}.pressure

# Run conditions

dump          4 all custom ${dtdump} ${project}.lammpstrj id type x y z

variable    pxy equal pxy
variable    pxz equal pxz
variable    pyz equal pyz
fix                sample_press all ave/time 1 1 50 v_pxy v_pxz v_pyz file ${project}.pressure

compute       7 liion msd
fix                 8 liion ave/time 1 1 ${dtdump} c_7[4] file liion_msd

compute assignchunk all chunk/atom molecule

compute allcom all com/chunk assignchunk
fix       20 all ave/time 1 1 ${dtdump} c_allcom[*] file all_com mode vector

compute msd all msd/chunk assignchunk
fix                 21 all ave/time 1 1 ${dtdump} c_msd[*] file msd_all mode vector

compute        22 all rdf 100 1 7*8 1 9 1 10
fix                 23 all ave/time 1 1 ${dtdump} c_22[*] file li_rdf mode vector

write_dump     liion custom liion_hop.dump id type x y z
variable       Dhop equal 4.0
variable       check atom "c_dsp[4] > v_Dhop"
compute        dsp liion displace/atom refresh check
dump          24 liion custom ${dtdump} liion_hop.dump id type x y z
dump_modify    24 append yes thresh c_dsp[4] > ${Dhop} &
            refresh c_dsp delay ${dtdump}
```

```
compute Rg backbone gyration/chunk assignchunk
fix 27 backbone ave/time 1 1 ${dtdump} c_Rg file pdms_gyration mode vector

compute coord liion coord/atom cutoff 3.0 7*8 9 10
dump 29 liion custom ${dtdump} li_coord id type c_coord[*]

compute cluster ion aggregate/atom 2.8
compute cc1 ion chunk/atom c_cluster compress yes
dump 30 ion custom ${dtdump} clusterid id type mass mol c_cc1

compute cluster2 mcoord cluster/atom 3.0
compute cc2 mcoord chunk/atom c_cluster2 compress yes
dump 31 mcoord custom ${dtdump} coordid id type mass mol c_cc2

compute com ion com/chunk cc1
fix       32 ion ave/time 1 1 ${dtdump} c_com[*] file cluster_com mode vector

restart 5000000 polymer.restart.*
restart           ${dtrestart} ${project}.restart1 ${project}.restart2
run               ${trun}
```

```
clear;clc;close all
f_dump=20000;  %10000;
timestep=0.5;  %fs
totalstep=160000000;  %20000000;
totaltime=timestep*totalstep*10^(-6); %ns
timeperframe=f_dump/totalstep*totaltime;
nframe=totalstep/f_dump+1;
n_atoms=340;
start=1;
data=readmatrix('clusterid');

alpha=repmat(zeros(25,25),1,1,nframe);
hist_avg=zeros(25,25);

% The size for count_everything has to be ...
% max{max(n_cluster),2+max(size(C2)) over all i and k}
count_everything=repmat(zeros(25,25),1,1,nframe);

for k=start:nframe

    clusterid=data(1+(n_atoms+9)*(k-1):n_atoms+(n_atoms+9)*(k-1),5);
    molid0=data(1+(n_atoms+9)*(k-1):n_atoms+(n_atoms+9)*(k-1),4);
    [C,ia,ic]=unique(clusterid);
    a_counts = accumarray(ic,1);

    value_counts = [C, a_counts];
    n_cluster=length(C);
count_everything(1:length(C),1:2,k)=[C, a_counts];

    for i=1:n_cluster
    index=find(clusterid==C(i));
    molid=molid0(index);
    [C2,ia2,ic2]=unique(molid);
```

```
    a_counts2 = accumarray(ic2,1);
    value_counts2 = [C2,a_counts2];

   % helpful to look at data file, identify the mol id range for cations and anions
    count_everything(i,3:2+length(C2),k)=C2;

    [C3,ia3,ic3]=unique(a_counts2);
    a_counts3 = accumarray(ic3,1);
    value_counts3 = [C3,a_counts3];
    if length(a_counts3)==1 && C3==1
        % free cations
        alpha(2,1,k)=alpha(2,1,k)+1;
    elseif length(a_counts3)==1 && C3==8
        % free anions
        alpha(1,2,k)=alpha(1,2,k)+1;

    %elseif length(a_counts3)==2 && a_counts3(1)==a_counts3(2)
        % neutral clusters (LiOTF OR Lin(OTF)n)
         %alpha(2,2,k)=alpha(2,2,k)+1;

    else
        % charged clusters
    alpha(a_counts3(1)+1,a_counts3(2)+1,k)=alpha(a_counts3(1)+1,a_counts3(2)+1,k)+1;
    end
    end
    hist_avg=alpha(:,:,k)+hist_avg;
end

%hist_data=alpha(:,:,1000)
hist_data=hist_avg/(nframe-start+1)
hist_data=hist_data(1:9,1:9)

x=0:8;
```

```
y=0:8;
grid on
imagesc(x,y,flipud(hist_data))
cc=colorbar;
cc.Ticks=linspace(0,20,5);
%cc.Label.String = '\fontsize{12} <\alpha_{ij}>';
set(cc.XLabel,{'String','Rotation','Position'},{'\fontsize{18} <\alpha_{ij}>',0,[0.5 26.0]})
colormap hot;
cmap = 1-colormap;
colormap(cmap);

ax = gca;
xt = ax.XTick;
yt = ax.YTick;
xt=[0 2 4 6 8];
yt=xt;
ax.XTickLabel = xt;
set(ax, 'YTick',yt, 'YTickLabel', flip(yt))
xlabel('n _')
ylabel('n_+')


hold on
hm = mesh(-0.5:1:8.5,-0.5:1:8.5,zeros([10 10]));
hm.FaceColor = 'none';
hm.EdgeColor = 'k';


hold on
%plot(-0.5:0.01:8.5,8.5:-0.01:-0.5,'r','Linewidth',1.5)

set(gca,'linewidth',1.0,'fontsize',18)
```

```
%{
ax = gca;
xt = ax.XTick;
yt = ax.YTick;
set(ax, 'XTick',0:9, 'XTickLabel', 0:9)
set(ax, 'YTick',0:9, 'YTickLabel', flip(0:9))
%}
```

```
close all;clear;clc

f_dump=20000;  %10000;
timestep=0.5;  %fs
totalstep=160000000;  %20000000;
totaltime=timestep*totalstep*10^(-6); %ns
timeperframe=f_dump/totalstep*totaltime;
nframe=totalstep/f_dump+1;
n_li=20;
start=1;% 15ns

data=readmatrix('cu_coord');
data_plot=repmat(zeros(n_li,4),1,1,(nframe-start+1));
coord_matrix=repmat(zeros(10,10),1,1,(nframe-start+1));
coord_sum=zeros(10,10);
for  k=start:nframe
data_plot(:,:,(k-start+1))=data(1+(n_li+9)*(k-1):n_li+(n_li+9)*(k-1),3:6);
for i=1:n_li
    n_N=data_plot(i,1,(k-start+1))+data_plot(i,2,(k-start+1));
    n_O=data_plot(i,3,(k-start+1));
    n_O2=data_plot(i,4,(k-start+1));
coord_matrix(n_O+1,n_N+1,(k-start+1))=coord_matrix(n_O+1,n_N+1,(k-start+1))+1;
end
coord_sum=coord_sum+coord_matrix(:,:,(k-start+1));
end
```

```
coord_sum=coord_sum/((nframe-start+1)*n_li) % probability for each coordination
combo
coord_sum=coord_sum(1:9,1:9)
x=0:8;
y=0:8;
grid on
imagesc(x,y,flipud(coord_sum))
cc=colorbar;
cc.Ticks=linspace(0,0.4,5);
set(cc.XLabel,{'String','Rotation','Position'},{'\fontsize{18} <p_{ij}>',0,[0.5 0.45]})
colormap hot;
cmap = 1-colormap;
colormap(cmap);



ax = gca;
xt = ax.XTick;
yt = ax.YTick;
xt=[0 2 4 6 8];
yt=xt;
ax.XTickLabel = xt;
set(ax, 'YTick',yt, 'YTickLabel', flip(yt))
xlabel('O_{PDMS}')
xlabel('N_{PI}')
ylabel('O_{OTf^-}')
```

```
hold on
hm = mesh(-0.5:1:8.5,-0.5:1:8.5,zeros([10 10]));
hm.FaceColor = 'none';
hm.EdgeColor = 'k';



hold on
%plot(-0.5:0.01:5.5,2.5:0.01:8.5,'color',[0.9290 0.6940 0.1250],'Linewidth',1.5)
hold on
plot(-0.5:0.01:6.5,1.5:0.01:8.5,'r','Linewidth',1.5)
%legend('','z_{total}=5','z_{total}=6','Location', 'Northeast',...
%    'FontSize',16);

legend('','z_{total}=6','Location', 'Northeast',...
    'FontSize',16);

set(gca,'linewidth',1.0,'fontsize',18)

figure()
bar3(flipud(coord_sum))
ax = gca;
xt = ax.XTick;
yt = ax.YTick;
ax.XTickLabel = xt-1;
set(ax, 'YTick',yt, 'YTickLabel', flip(yt-1))
xlabel('N_{Pl}')
```

```
ylabel('O_{OTF}')
zlabel('Probability Mass')
set(gca,'linewidth',1.0,'fontsize',16)
```

```
clear all;close all;clc

data=readmatrix('all_com');
x=data(:,2);
y=data(:,3);
z=data(:,4);
n_windows=75;
msd=repmat(zeros(1,1001),1,1,n_windows);
msd_ave=zeros(1,1001);
start_window=1;
for k=start_window:n_windows
    index_origin=61+(k-1)*81*100;
    index_end=80+(k-1)*81*100;
for i=1:1001

    dx=x((index_origin+81*(i-1)):(index_end+81*(i-1)))-x(index_origin:index_end);
    dy=y((index_origin+81*(i-1)):(index_end+81*(i-1)))-y(index_origin:index_end);
    dz=z((index_origin+81*(i-1)):(index_end+81*(i-1)))-z(index_origin:index_end);
    msd0=dx.^2+dy.^2+dz.^2;
    msd(1,i,k)=sum(msd0)/20;
end
    msd_ave=msd(:,:,k)+msd_ave;
end

time=linspace(0,10,1001);
plot(time,msd_ave/(n_windows-start_window+1),'color',[0.8500 0.3250
0.0980],'Linewidth',3)
```

```
hold on
msd_cu=msd_ave/(n_windows-start_window+1);
D_cu=time'\(msd_ave/(n_windows-start_window+1))';
D_cu=D_cu/6;

msd2=repmat(zeros(1,1001),1,1,n_windows);
msd_ave2=zeros(1,1001);
for k=start_window:n_windows
    index_origin=21+(k-1)*81*100;
    index_end=60+(k-1)*81*100;
for i=1:1001
    dx2=x((index_origin+81*(i-1)):(index_end+81*(i-1)))-x(index_origin:index_end);
    dy2=y((index_origin+81*(i-1)):(index_end+81*(i-1)))-y(index_origin:index_end);
    dz2=z((index_origin+81*(i-1)):(index_end+81*(i-1)))-z(index_origin:index_end);
    msd0=dx2.^2+dy2.^2+dz2.^2;
    msd2(1,i,k)=sum(msd0)/40;
end
    msd_ave2=msd2(:,:,k)+msd_ave2;
end

time=linspace(0,10,1001);
plot(time,msd_ave2/(n_windows-start_window+1),'color',[0.4660 0.6740
0.1880],'Linewidth',3)
msd_otf=msd_ave2/(n_windows-start_window+1);
D_otf=time'\(msd_ave2/(n_windows-start_window+1))';
D_otf=D_otf/6;
```

```
msd3=repmat(zeros(1,1001),1,1,n_windows);
msd_ave3=zeros(1,1001);
for k=start_window:n_windows
    index_origin=1+(k-1)*81*100;
    index_end=20+(k-1)*81*100;
for i=1:1001
    dx3=x((index_origin+81*(i-1)):(index_end+81*(i-1)))-x(index_origin:index_end);
    dy3=y((index_origin+81*(i-1)):(index_end+81*(i-1)))-y(index_origin:index_end);
    dz3=z((index_origin+81*(i-1)):(index_end+81*(i-1)))-z(index_origin:index_end);
    msd0=dx3.^2+dy3.^2+dz3.^2;
    msd3(1,i,k)=sum(msd0)/20;
end
    msd_ave3=msd3(:,:,k)+msd_ave3;
end


time=linspace(0,10,1001);
plot(time,msd_ave3/(n_windows-start_window+1),'color',[0.9290 0.6940
0.1250],'Linewidth',3)
D_chain=time'\(msd_ave3/(n_windows-start_window+1))';
D_chain=D_chain/6;
msd_chain=msd_ave3/(n_windows-start_window+1);


xlabel('Time (ns)')
Ang = char(197);
```

```
ylabel(['MSD (' Ang '^2)'])
set(gca,'linewidth',1.0,'fontsize',18)
legend('Cu^{2+}','OTf-','P-PI','Location', 'Northwest','FontSize',16);


n_ion=20;
V=68432.109*10^(-30);
p=n_ion/V;
q=1.60217662*10^(-19);
q_cu=2*q;
q_otf=q;
p_cu=p;
p_otf=2*p;
k=1.38064852*10^(-23);
T=303;
D_cu=D_cu*10^(-11);
D_otf=D_otf*10^(-11); % m/s
%D_chain=D_chain*10^(-11);
sigma=q_cu^2*p_cu*D_cu/(k*T)+q_otf^2*p_otf*D_otf/(k*T); % S/m
%sigma_c=q^2/(V*k*T)*10^(-
11)*(4*3.9807*0.1386+14.7075*0.5361+5.4646*0.3423+4*0.3498*0.3695+0.4804*0.188
8+0.5146*0.4970);
%sigma_c=q^2/(V*k*T)*10^(-11)*(0.5146*0.4970);
fprintf('The calculated NE ionic conductivity (in S/m) equals %f\n',sigma)
```

```
close all;clear;clc

f_dump=20000;  %10000;
timestep=0.5;  %fs
totalstep=160000000;  %20000000;
totaltime=timestep*totalstep*10^(-6); %ns
timeperframe=f_dump/totalstep*totaltime;
nframe=totalstep/f_dump+1;
n_total=220;
selected_index= 5386;     %5225;

data=readmatrix('coordid');
%data_info=repmat(zeros(n_total,5),1,1,nframe);
for  k=1:nframe
%data_info(:,:,k)=data(1+(n_total+9)*(k-1):n_total+(n_total+9)*(k-1),1:5);
atomid=data(1+(n_total+9)*(k-1):n_total+(n_total+9)*(k-1),1);
atomrow=find(atomid==selected_index);
clusterid=data(1+(n_total+9)*(k-1):n_total+(n_total+9)*(k-1),5);
locatecluster=clusterid(atomrow);
coordrow=find(clusterid==locatecluster);
coordrow=coordrow(coordrow~=atomrow);
coordid=atomid(coordrow);
curtime=timeperframe*(k-1)*ones(length(coordid),1);
plot(curtime,coordid,'o','MarkerEdgeColor','k','MarkerFaceColor','b','MarkerSize',6)
hold on
end
```

```
yline(5061,'r-','linewidth',1.0)
hold on
yline(5381,'r-','linewidth',1.0)
ylim([0 5500])
set(gca,'linewidth',1.0,'fontsize',18)
xlim([0 85])

for j=1:20
    hold on
    if j<20
    yline(j*253,'k--',num2str(j),'LabelVerticalAlignment','bottom')
    else
        yline(5061,'k--','20','LabelVerticalAlignment','bottom','linewidth',1.0)
    end

end
ylabel('Coordination index')
xlabel('Time (ns)')
```

```
# LAMMPS input script for standardized atomistic simulations
# Created by emc_setup.pl v4.1, August 1, 2021 as part of EMC
# on Wed Apr 27 13:21:26 EDT 2022

# LAMMPS atomistic input script

echo            screen
units           real
atom_style      full
boundary p p p

# Variable definitions

variable        project         index   "polymer"       # project name
variable        source          index   .       # data directory
variable        params          index   .       # parameter directory
variable        temperature     index   303             # system temperature
variable        tdamp           index   50              # temperature damping
variable        pdamp           index   500       # pressure damping
variable        dielectric      index   1.0             # medium dielectric
variable        kappa           index   4               # electrostatics kappa
variable        cutoff          index   12.0            # standard cutoff
variable        charge_cutoff   index   12.0            # charge cutoff
variable        precision       index   0.00001                 # kspace precision
variable        lseed           index   723853                  # langevin seed
variable        vseed           index   486234                  # velocity seed
variable        tequil          index   10000000        # equilibration time
variable        dlimit          index   0.1             # nve/limit distance
variable        trun            index   10000000                # run time
variable        frestart        index   1               # 0: equil, 1: restart
variable        dtrestart       index   5000            # delta restart time
variable        dtdump          index   5000            # delta dump time
variable        dtthermo        index   5000            # delta thermo time
variable        timestep        index   0.5             # integration time step
variable        tfreq           index   50              # profile sampling freq
variable        nsample         index   400             # profile conf sampling
variable        dtime           equal   ${tfreq}*${nsample}   # profile dtime
variable        restart         index   ${params}/${project}.restarteq

if "${frestart} != 0" then &
"variable       data            index   ${restart}" &
else &
"variable       data            index   ${params}/${project}.data" &
```

```
# Interaction potential definition

pair_style lj/class2/coul/cut ${cutoff} ${charge_cutoff}
bond_style      class2
angle_style     class2
dihedral_style class2
improper_style          class2
pair_modify     mix sixthpower tail yes
special_bonds lj/coul 0 0 1

if "${frestart} != 0" then "read_restart ${data}" else "read_data ${data}"
include         ${params}/${project}.params

neighbor 2.0 bin
neigh_modify  delay 0 every 1 check yes

# Integration conditions (check)
timestep        ${timestep}
dielectric      ${dielectric}
fix             mom all momentum ${dtdump} linear 1 1 1 angular

#if "${frestart} != 0" then "jump SELF simulate"

group liion type 1
group otfion molecule 21:40
group backbone molecule 1:20
group ion union liion otfion


# Minimization
#fix min all box/relax aniso 0.0 vmax 0.001
#min_style sd 1e-5
#minimize 1e-25 1e-25 5000 10000

#min_style cg 1e-5
#minimize 1e-25 1e-25 5000 10000
#unfix min

# specify initial velocity of atoms
#velocity        all create ${temperature} ${vseed} &
#               dist gaussian rot yes mom yes sum yes
#run 0
#velocity        all scale ${temperature} dist gaussian rot yes mom yes sum yes
```

```
#reset_timestep 0
thermo                  ${dtthermo}
thermo_style custom step temp pe etotal lx ly lz vol density press pxx pyy pzz
dump        1 all custom 5000 equilibration3.lammpstrj id type x y z

# constant room temp
#fix nvt_eq all nvt temp ${temperature} ${temperature} ${tdamp}
#restart       ${dtrestart} ${project}.restarteq1 ${project}.restarteq2
#run 3000000
#unfix nvt_eq
#unfix mom

#room temp and pressure
#fix npt2 all npt temp ${temperature} ${temperature} ${tdamp} aniso 1.0 1.0 ${pdamp} drag 0.2
#restart       ${dtrestart} ${project}.restarteq1 ${project}.restarteq2
#run 2000000
#unfix npt2

fix nvt_eq2 all nvt temp ${temperature} ${temperature} ${tdamp}
restart       ${dtrestart} ${project}.restarteq1 ${project}.restarteq2
run 3000000
unfix nvt_eq2

undump 1
write_restart   ${project}.restarteq

# Simulation

label           simulate

# Integrator
reset_timestep 0
thermo                  ${dtthermo}

pair_style lj/class2/coul/long ${cutoff} ${charge_cutoff}
bond_style      class2
angle_style     class2
dihedral_style class2
improper_style          class2
pair_modify     mix sixthpower tail yes
special_bonds lj/coul 0 0 1

include         ${params}/${project}.params
```

```
kspace_style pppm/cg ${precision}


#variable       srate equal 5e-14               # velocity of top edge
#variable       xyrate equal ${srate}/ly
#variable xyrate equal 2e-13
variable xyrate equal 1e-6

unfix mom
fix             1 all nvt/sllod temp ${temperature} ${temperature} ${tdamp}
fix             2 all deform 1 xy erate ${xyrate} remap v

compute             usual all temp
compute             tilt all temp/deform

thermo_style  custom step temp c_usual etotal press pxy ly
thermo_modify       temp tilt

run 1000000

# Run conditions

#variable       visc equal -pxy/(v_srate/ly)
variable        visc equal -pxy/v_xyrate
fix             vave all ave/time 100 10 1000 v_visc ave running start 1000000 file
${project}.viscosity
fix             sample_press all ave/time 1 1 100 v_visc file ${project}.pressure

thermo_style  custom step temp press pxy ly v_visc f_vave
thermo_modify       temp tilt

restart         ${dtrestart} ${project}.restart1 ${project}.restart2
run             ${trun}
```

```
clear;clc;close all
Ndump=2000;
Nevery=5;
Nrepeat=Ndump/Nevery;
totaltimesteps=100000;

value_timestep=0:Nevery:Ndump;
delta=0:Nevery:(Nrepeat-1)*Nevery;
N_samples0=(Nrepeat+1):-1:2;
N_samples=Nrepeat*(totaltimesteps/Ndump-1)+N_samples0;

data=readmatrix('polymer_pressure');
Pxy=zeros(1,Nrepeat);
Pxy(1)=sum((data(:,2)).^2);
Pxz=zeros(1,Nrepeat);
Pxz(1)=sum((data(:,3)).^2);
Pyz=zeros(1,Nrepeat);
Pyz(1)=sum((data(:,4)).^2);

for i=2:Nrepeat
    for j=1:N_samples(i)
    increment_xy=data(j,2)*data(j+delta(i)/Nevery,2);
    Pxy(i)=Pxy(i)+increment_xy;
    increment_xz=data(j,3)*data(j+delta(i)/Nevery,3);
    Pxz(i)=Pxz(i)+increment_xz;
    increment_yz=data(j,4)*data(j+delta(i)/Nevery,4);
    Pyz(i)=Pyz(i)+increment_yz;
```

```
    end
end
Pxy=Pxy./N_samples;
Pxz=Pxz./N_samples;
Pyz=Pyz./N_samples;

% T=  %K
% kB= 1.3806504e-23    %[J/K]
% V=vol  %A^3
% dt=   %fs
% Nevery  %unitless
% scale=convert/(kB*T)*V*Nevery*dt;
%T=303;  %K
%kB= 1.3806504e-23;    %[J/K]
%V=66940.521; %A^3
%dt=0.5;  %fs
%convert=1.0266755625e-35;
%scale=convert/(kB*T)*V*Nevery*dt;
scale=1.70979182368186e-09;
v11=(0.5*(Pxy(1)+Pxy(end))+sum(Pxy(2:end-1)))*scale;
v22=(0.5*(Pxz(1)+Pxz(end))+sum(Pxz(2:end-1)))*scale;
v33=(0.5*(Pyz(1)+Pyz(end))+sum(Pyz(2:end-1)))*scale;
miu=(v11+v22+v33)/3
```

```
; RUN CONTROL PARAMETERS
integrator              = md
tinit                   = 0             ; Start time and timestep in ps
dt                      = 0.020         ; Timestep in ps
nsteps                  = 2000000
simulation_part         = 1
init_step               = 0
comm-mode               = Linear        ; mode for center of mass motion removal
nstcomm                 = 100           ; number of steps for center of mass motion removal
comm-grps               =               ; group(s) for center of mass motion removal


; LANGEVIN DYNAMICS OPTIONS
bd-fric                 = 0             ; Friction coefficient (amu/ps)
ld_seed                 = 1347          ; random seed


; OUTPUT CONTROL OPTIONS
nstxout                 = 1000          ; Output frequency for coords (x)
nstvout                 = 1000          ; Output frequency for velocities (v)
nstfout                 = 0             ; Output frequency for forces (f)
nstlog                  = 1000          ; Output frequency for energies to log file
nstenergy               = 1000          ; Output frequency for energies to energy file
nstxtcout               = 1000          ; Output frequency for xtc file
xtc-precision           = 100           ; Precision for xtc file


; NEIGHBORSEARCHING PARAMETERS
nstlist                 = 5             ; nblist update frequency
ns_type                 = grid          ; ns algorithm (simple or grid)
pbc                     = xyz           ; Periodic boundary conditions: xyz, no, xy
periodic_molecules      = no
rlist                   = 1.2           ; nblist cut-off


; OPTIONS FOR ELECTROSTATICS AND VDW
coulombtype             = PME           ; Method for doing electrostatics, originally Shift. PME can
also be used with the polariable model
rcoulomb-switch         = 0.
rcoulomb                = 1.2           ; 1.2 for Switch; 1.5 for PME is recommended but requires
changing rlist (to which the system is very sensitve)
epsilon_r               = 2.5           ; Relative dielectric constant for the medium

vdw-type                = Shift         ; Method for doing Van der Waals
```

```
rvdw-switch      = 0.9
rvdw             = 1.2
DispCorr         = No        ; Apply long range dispersion corrections for Energy and Pressure
table-extension  = 1         ; Extension of the potential lookup tables beyond the cut-off
energygrp_table  =           ; Seperate tables between energy group pairs
fourierspacing   = 0.12      ; Spacing for the PME/PPPM FFT grid
fourier_nx       = 0         ; FFT grid size, when a value is 0 fourierspacing will be used
fourier_ny       = 0         ;  - " -
fourier_nz       = 0         ;  - " -
pme_order        = 4         ; EWALD/PME/PPPM parameters
ewald_rtol       = 1e-05     ;  - " -
ewald_geometry   = 3d        ;  - " -
epsilon_surface  = 0         ;  - " -
optimize_fft     = no        ;  - " -


; IMPLICIT SOLVENT ALGORITHM
implicit_solvent  = No


; OPTIONS FOR WEAK COUPLING ALGORITHMS
Tcoupl           = v-rescale ; Temperature coupling: berendsen, v-rescale
tc-grps          = System    ; Groups to couple separately
tau_t            = 1.0       ; Time constant (ps)
ref_t            = 298       ; Reference temperature (K)

Pcoupl           = Parrinello-Rahman ; Pressure coupling: no, Berendsen, Parrinello-Rahman
Pcoupltype       = semiisotropic    ;
tau-p            = 5.0       ; Time constant (ps)
compressibility  = 0.0 3e-5          ; Compressibility (1/bar)
ref-p            = 1.0 1.0           ; Reference P (bar)

refcoord_scaling  = No       ; Scaling of reference coordinates, No, All or COM
andersen_seed     = 814141   ; Random seed for Andersen thermostat


; GENERATE VELOCITIES FOR STARTUP RUN
gen_vel          = no
gen-temp         = 298
gen-seed         = 173510
```

```
; OPTIONS FOR BONDS
constraints            = none
constraint-algorithm     = Lincs          ; Type of constraint algorithm
continuation           = no               ; Do not constrain the start configuration
Shake-SOR              = no               ; Use successive overrelaxation to reduce the number of
shake iterations
shake-tol              = 0.0001     ; Relative tolerance of shake
lincs-order            = 4          ; Highest order in the expansion of the constraint coupling matrix
lincs-iter             = 1          ; Number of iterations in the final step of LINCS. 1 is fine for
                                          ; normal simulations, but use 2 to conserve energy in NVE
runs.
                                          ; For energy minimization with constraints it should be 4 to
8.
lincs-warnangle        = 30               ; Lincs will write a warning to the stderr if in one step a
bond
                                          ; rotates over more degrees than
morse                  = no          ; Convert harmonic bonds to morse potentials


; Free energy control stuff
free-energy            = no
init-lambda            = 0
delta-lambda           = 0
sc-alpha               = 0
sc-power               = 0
sc-sigma               = 0.3
couple-moltype         =
couple-lambda0         = vdw-q
couple-lambda1         = vdw-q
couple-intramol        = no
```

BIBLIOGRAPHY

[1] J. N. Canongia Lopes and A. A. Pádua, "Molecular force field for ionic liquids composed of triflate or bistriflylimide anions," *The Journal of Physical Chemistry B*, vol. 108, no. 43, pp. 16893–16898, 2004.

[2] A. France-Lanord and J. C. Grossman, "Correlations from ion pairing and the nernst-einstein equation," *Physical review letters*, vol. 122, no. 13, p. 136001, 2019.

[3] X. Zhang, J. Dai, M. Tepermeister, Y. Deng, J. Yeo, and M. N. Silberstein, "Understanding how metal–ligand coordination enables solvent free ionic conductivity in pdms," *Macromolecules*, vol. 56, no. 8, pp. 3119–3131, 2023.

[4] O. J. Cayre, S. T. Chang, and O. D. Velev, "Polyelectrolyte diode: nonlinear current response of a junction between aqueous ionic gels," *Journal of the American Chemical Society*, vol. 129, no. 35, pp. 10801–10806, 2007.

[5] R. Agrawal and G. Pandey, "Solid polymer electrolytes: materials designing and all-solid-state battery applications: an overview," *Journal of Physics D: Applied Physics*, vol. 41, no. 22, p. 223001, 2008.

[6] B. Smitha, S. Sridhar, and A. Khan, "Solid polymer electrolyte membranes for fuel cell applications—a review," *Journal of membrane science*, vol. 259, no. 1-2, pp. 10–26, 2005.

[7] M. Armand, "Polymers with ionic conductivity," *Advanced Materials*, vol. 2, no. 6-7, pp. 278–286, 1990.

[8] Y. Jiang, X. Yan, Z. Ma, P. Mei, W. Xiao, Q. You, and Y. Zhang, "Development of the peo based solid polymer electrolytes for all-solid state lithium ion batteries," *Polymers*, vol. 10, no. 11, p. 1237, 2018.

[9] H. Ohno, M. Yoshizawa, and W. Ogihara, "Development of new class of ion conductive polymers based on ionic liquids," *Electrochimica Acta*, vol. 50, no. 2-3, pp. 255–261, 2004.

[10] W. Qian, J. Texter, and F. Yan, "Frontiers in poly (ionic liquid) s: syntheses and applications," *Chemical Society Reviews*, vol. 46, no. 4, pp. 1124–1159, 2017.

[11] B. Bhandari, G.-Y. Lee, and S.-H. Ahn, "A review on ipmc material as actuators and sensors: fabrications, characteristics and applications," *International journal of precision engineering and manufacturing*, vol. 13, no. 1, pp. 141–163, 2012.

[12] J. Zhu, Z. Zhang, S. Zhao, A. S. Westover, I. Belharouak, and P.-F. Cao, "Single-ion conducting polymer electrolytes for solid-state lithium–metal batteries: design, performance, and challenges," *Advanced Energy Materials*, vol. 11, no. 14, p. 2003836, 2021.

[13] J. Wang, D. Gao, and P. S. Lee, "Recent progress in artificial muscles for interactive soft robotics," *Advanced Materials*, vol. 33, no. 19, p. 2003088, 2021.

[14] S. Ma, Y. Zhang, Y. Liang, L. Ren, W. Tian, and L. Ren, "High-performance ionic-polymer–metal composite: toward large-deformation fast-response artificial muscles," *Advanced Functional Materials*, vol. 30, no. 7, p. 1908508, 2020.

[15] K. Xiao, C. Wan, L. Jiang, X. Chen, and M. Antonietti, "Bioinspired ionic sensory systems: the successor of electronics," *Advanced Materials*, vol. 32, no. 31, p. 2000218, 2020.

[16] M. Tepermeister, N. Bosnjak, J. Dai, X. Zhang, S. M. Kielar, Z. Wang, Z. Tian, J. Suntivich, and M. N. Silberstein, "Soft ionics: Governing physics and state of technologies," *Frontiers in Physics*, p. 453, 2022.

[17] D. J. Brooks, B. V. Merinov, W. A. Goddard III, B. Kozinsky, and J. Mailoa, "Atomistic description of ionic diffusion in peo–litfsi: Effect of temperature, molecular weight, and ionic concentration," *Macromolecules*, vol. 51, no. 21, pp. 8987–8995, 2018.

[18] N. Molinari, J. P. Mailoa, and B. Kozinsky, "Effect of salt concentration on ion clustering and transport in polymer solid electrolytes: a molecular dynamics study of peo–litfsi," *Chemistry of Materials*, vol. 30, no. 18, pp. 6298–6306, 2018.

[19] K.-H. Shen, M. Fan, and L. M. Hall, "Molecular dynamics simulations of ion-containing polymers using generic coarse-grained models," *Macromolecules*, vol. 54, no. 5, pp. 2031–2052, 2021.

[20] T. Sedghamiz, A. Y. Mehandzhiyski, M. Modarresi, M. Linares, and I. Zozoulenko, "What can we learn about pedot: Pss morphology from molecular dynamics simulations of ionic diffusion?," *Chemistry of Materials*, 2023.

[21] K. Laasonen and M. L. Klein, "Molecular dynamics simulations of the structure and ion diffusion in poly (ethylene oxide)," *Journal of the Chemical Society, Faraday Transactions*, vol. 91, no. 16, pp. 2633–2638, 1995.

[22] Y. Ding, J. Zhang, L. Chang, X. Zhang, H. Liu, and L. Jiang, "Preparation of high-performance ionogels with excellent transparency, good mechanical strength, and high conductivity," *Advanced Materials*, vol. 29, no. 47, p. 1704253, 2017.

[23] Y. Wu, S. Joseph, and N. Aluru, "Effect of cross-linking on the diffusion of water, ions, and small molecules in hydrogels," *The Journal of Physical Chemistry B*, vol. 113, no. 11, pp. 3512–3520, 2009.

[24] G. E. Sanoja, N. S. Schauser, J. M. Bartels, C. M. Evans, M. E. Helgeson, R. Seshadri, and R. A. Segalman, "Ion transport in dynamic polymer networks based on metal–ligand coordination: effect of cross-linker concentration," *Macromolecules*, vol. 51, no. 5, pp. 2017–2026, 2018.

[25] S. D. Jones, N. S. Schauser, G. H. Fredrickson, and R. A. Segalman, "The role of polymer–ion interaction strength on the viscoelasticity and conductivity of solvent-free polymer electrolytes," *Macromolecules*, vol. 53, no. 23, pp. 10574–10581, 2020.

[26] N. S. Schauser, G. E. Sanoja, J. M. Bartels, S. K. Jain, J. G. Hu, S. Han, L. M. Walker, M. E. Helgeson, R. Seshadri, and R. A. Segalman, "Decoupling bulk mechanics and mono-and multivalent ion transport in polymers based on metal–ligand coordination," *Chemistry of Materials*, vol. 30, no. 16, pp. 5759–5769, 2018.

[27] Y. Cao, T. G. Morrissey, E. Acome, S. I. Allec, B. M. Wong, C. Keplinger, and C. Wang, "A transparent, self-healing, highly stretchable ionic conductor," *Advanced Materials*, vol. 29, no. 10, p. 1605099, 2017.

[28] R. Li, T. Fan, G. Chen, K. Zhang, B. Su, J. Tian, and M. He, "Autonomous

self-healing, antifreezing, and transparent conductive elastomers," *Chemistry of Materials*, vol. 32, no. 2, pp. 874–881, 2020.

[29] J. Zhao, J. Gong, G. Wang, K. Zhu, K. Ye, J. Yan, and D. Cao, "A self-healing hydrogel electrolyte for flexible solid-state supercapacitors," *Chemical Engineering Journal*, vol. 401, p. 125456, 2020.

[30] P. Janson, E. O. Gabrielsson, K. J. Lee, M. Berggren, and D. T. Simon, "An ionic capacitor for integrated iontronic circuits," *Advanced Materials Technologies*, vol. 4, no. 4, p. 1800494, 2019.

[31] S. T. Martin, A. Akbari, P. C. Banerjee, A. Neild, and M. Majumder, "The inside-out supercapacitor: induced charge storage in reduced graphene oxide," *Physical Chemistry Chemical Physics*, vol. 18, no. 47, pp. 32185–32191, 2016.

[32] K. Tybrandt, K. C. Larsson, A. Richter-Dahlfors, and M. Berggren, "Ion bipolar junction transistors," *Proceedings of the National Academy of Sciences*, vol. 107, no. 22, pp. 9929–9932, 2010.

[33] K. Tybrandt, E. O. Gabrielsson, and M. Berggren, "Toward complementary ionic circuits: The npn ion bipolar junction transistor," *Journal of the American Chemical Society*, vol. 133, no. 26, pp. 10141–10145, 2011.

[34] E. O. Gabrielsson, K. Tybrandt, and M. Berggren, "Polyphosphonium-based ion bipolar junction transistors," *Biomicrofluidics*, vol. 8, no. 6, 2014.

[35] N. Boon and M. O. De La Cruz, "'soft'amplifier circuits based on field-effect ionic transistors," *Soft Matter*, vol. 11, no. 24, pp. 4793–4798, 2015.

[36] C. Zhong, Y. Deng, A. F. Roudsari, A. Kapetanovic, M. Anantram, and

M. Rolandi, "A polysaccharide bioprotonic field-effect transistor," *Nature communications*, vol. 2, no. 1, p. 476, 2011.

[37] M. Hao, Y. Wang, Z. Zhu, Q. He, D. Zhu, and M. Luo, "A compact review of ipmc as soft actuator and sensor: current trends, challenges, and potential solutions from our recent work," *Frontiers in Robotics and AI*, vol. 6, p. 129, 2019.

[38] H. J. Kim, B. Chen, Z. Suo, and R. C. Hayward, "Ionoelastomer junctions between polymer networks of fixed anions and cations," *Science*, vol. 367, no. 6479, pp. 773–776, 2020.

[39] Z. Cao, H. Liu, and L. Jiang, "Transparent, mechanically robust, and ultrastable ionogels enabled by hydrogen bonding between elastomers and ionic liquids," *Materials Horizons*, vol. 7, no. 3, pp. 912–918, 2020.

[40] E. O. Gabrielsson, P. Janson, K. Tybrandt, D. T. Simon, and M. Berggren, "A four-diode full-wave ionic current rectifier based on bipolar membranes: Overcoming the limit of electrode capacity," *Advanced Materials*, vol. 26, no. 30, pp. 5143–5147, 2014.

[41] C. Wang, K. Fu, J. Dai, S. D. Lacey, Y. Yao, G. Pastel, L. Xu, J. Zhang, and L. Hu, "Inverted battery design as ion generator for interfacing with biosystems," *Nature communications*, vol. 8, no. 1, p. 15609, 2017.

[42] S. Y. Yeon, J. Yun, S.-h. Yoon, D. Lee, W. Jang, S. H. Han, C. M. Kang, and T. D. Chung, "A miniaturized solid salt reverse electrodialysis battery: a durable and fully ionic power source," *Chemical Science*, vol. 9, no. 42, pp. 8071–8076, 2018.

[43] S. Kim, S. J. Choi, K. Zhao, H. Yang, G. Gobbi, S. Zhang, and J. Li, "Electrochemically driven mechanical energy harvesting," *Nature communications*, vol. 7, no. 1, p. 10146, 2016.

[44] H. Wang, D. Zhao, Z. U. Khan, S. Puzinas, M. P. Jonsson, M. Berggren, and X. Crispin, "Ionic thermoelectric figure of merit for charging of supercapacitors," *Advanced Electronic Materials*, vol. 3, no. 4, p. 1700013, 2017.

[45] N. S. Schauser, R. Seshadri, and R. A. Segalman, "Multivalent ion conduction in solid polymer systems," *Molecular Systems Design & Engineering*, vol. 4, no. 2, pp. 263–279, 2019.

[46] J.-H. Shin, W. A. Henderson, and S. Passerini, "Ionic liquids to the rescue? overcoming the ionic conductivity limitations of polymer electrolytes," *Electrochemistry Communications*, vol. 5, no. 12, pp. 1016–1020, 2003.

[47] J. Imbrogno, K. Maruyama, F. Rivers, J. R. Baltzegar, Z. Zhang, P. W. Meyer, V. Ganesan, S. Aoshima, and N. A. Lynd, "Relationship between ionic conductivity, glass transition temperature, and dielectric constant in poly (vinyl ether) lithium electrolytes," *ACS Macro Letters*, vol. 10, no. 8, pp. 1002–1007, 2021.

[48] K.-H. Shen and L. M. Hall, "Effects of ion size and dielectric constant on ion transport and transference number in polymer electrolytes," *Macromolecules*, vol. 53, no. 22, pp. 10086–10096, 2020.

[49] R. J. Wojtecki, M. A. Meador, and S. J. Rowan, "Using the dynamic bond to access macroscopically responsive structurally dynamic polymers," *Nature materials*, vol. 10, no. 1, pp. 14–27, 2011.

[50] S. C. Grindy, R. Learsch, D. Mozhdehi, J. Cheng, D. G. Barrett, Z. Guan, P. B. Messersmith, and N. Holten-Andersen, "Control of hierarchical polymer mechanics with bioinspired metal-coordination dynamics," *Nature materials*, vol. 14, no. 12, pp. 1210–1216, 2015.

[51] C.-H. Li and J.-L. Zuo, "Self-healing polymers based on coordination bonds," *Advanced Materials*, vol. 32, no. 27, p. 1903762, 2020.

[52] E. Khare, N. Holten-Andersen, and M. J. Buehler, "Transition-metal coordinate bonds for bioinspired macromolecules with tunable mechanical properties," *Nature Reviews Materials*, vol. 6, no. 5, pp. 421–436, 2021.

[53] X. Zhang, Y. Vidavsky, S. Aharonovich, S. J. Yang, M. R. Buche, C. E. Diesendruck, and M. N. Silberstein, "Bridging experiments and theory: isolating the effects of metal–ligand interactions on viscoelasticity of reversible polymer networks," *Soft Matter*, vol. 16, no. 37, pp. 8591–8601, 2020.

[54] X. Zhang, R. Crisci, J. A. Finlay, H. Cai, A. S. Clare, Z. Chen, and M. N. Silberstein, "Enabling tunable water-responsive surface adaptation of pdms via metal–ligand coordinated dynamic networks," *Advanced Materials Interfaces*, vol. 9, no. 15, p. 2200430, 2022.

[55] H.-N. Wang, X. Meng, L.-Z. Dong, Y. Chen, S.-L. Li, and Y.-Q. Lan, "Coordination polymer-based conductive materials: ionic conductivity vs. electronic conductivity," *Journal of Materials Chemistry A*, vol. 7, no. 42, pp. 24059–24091, 2019.

[56] N. S. Schauser, D. J. Grzetic, T. Tabassum, G. A. Kliegle, M. L. Le, E. M. Susca, S. Antoine, T. J. Keller, K. T. Delaney, S. Han, *et al.*, "The role of

backbone polarity on aggregation and conduction of ions in polymer electrolytes," *Journal of the American Chemical Society*, vol. 142, no. 15, pp. 7055–7065, 2020.

[57] E. B. Anderson and T. E. Long, "Imidazole-and imidazolium-containing polymers for biology and material science applications," *Polymer*, vol. 51, no. 12, pp. 2447–2454, 2010.

[58] A. Nikolaev, P. M. Richardson, S. Xie, L. Canzian Llanes, S. D. Jones, O. Nordness, H. Wang, G. C. Bazan, R. A. Segalman, R. J. Clément, *et al.*, "Role of electron-deficient imidazoles in ion transport and conductivity in solid-state polymer electrolytes," *Macromolecules*, vol. 55, no. 3, pp. 971–977, 2022.

[59] W. Zhou, Z. Wang, Y. Pu, Y. Li, S. Xin, X. Li, J. Chen, and J. B. Goodenough, "Double-layer polymer electrolyte for high-voltage all-solid-state rechargeable batteries," *Advanced Materials*, vol. 31, no. 4, p. 1805574, 2019.

[60] G. Lu, H. Qiu, X. Du, K. K. Sonigara, J. Wang, Y. Zhang, Z. Chen, L. Chen, Y. Ren, Z. Zhao, *et al.*, "Heteroleptic coordination polymer electrolytes initiated by lewis-acidic eutectics for solid zinc–metal batteries," *Chemistry of Materials*, vol. 34, no. 19, pp. 8975–8986, 2022.

[61] B. Dünweg and K. Kremer, "Molecular dynamics simulation of a polymer chain in solution," *The Journal of chemical physics*, vol. 99, no. 9, pp. 6983–6997, 1993.

[62] N. Boden, S. Leng, and I. Ward, "Ionic conductivity and diffusivity in polyethylene oxode/electrolyte solutions as models for polymer electrolytes," *Solid State Ionics*, vol. 45, no. 3-4, pp. 261–270, 1991.

[63] D. R. Wheeler and J. Newman, "Molecular dynamics simulations of multicomponent diffusion. 1. equilibrium method," *The Journal of Physical Chemistry B*, vol. 108, no. 47, pp. 18353–18361, 2004.

[64] J. Wang and T. Hou, "Application of molecular dynamics simulations in molecular property prediction ii: diffusion coefficient," *Journal of computational chemistry*, vol. 32, no. 16, pp. 3505–3519, 2011.

[65] P. J. in't Veld and G. C. Rutledge, "Temperature-dependent elasticity of a semicrystalline interphase composed of freely rotating chains," *Macromolecules*, vol. 36, no. 19, pp. 7358–7365, 2003.

[66] H. Sun, "Force field for computation of conformational energies, structures, and vibrational frequencies of aromatic polyesters," *Journal of Computational Chemistry*, vol. 15, no. 7, pp. 752–768, 1994.

[67] I. Leontyev and A. Stuchebrukhov, "Accounting for electronic polarization in non-polarizable force fields," *Physical Chemistry Chemical Physics*, vol. 13, no. 7, pp. 2613–2626, 2011.

[68] S. Naserifar, D. J. Brooks, W. A. Goddard III, and V. Cvicek, "Polarizable charge equilibration model for predicting accurate electrostatic interactions in molecules and solids," *The Journal of chemical physics*, vol. 146, no. 12, p. 124117, 2017.

[69] D. Bedrov, J.-P. Piquemal, O. Borodin, A. D. MacKerell Jr, B. Roux, and C. Schroder, "Molecular dynamics simulations of ionic liquids and electrolytes using polarizable force fields," *Chemical reviews*, vol. 119, no. 13, pp. 7940–7995, 2019.

[70] Z. Xiong, Y. Liu, and H. Sun, "Electrostatic and covalent contributions in the coordination bonds of transition metal complexes," *The Journal of Physical Chemistry A*, vol. 112, no. 11, pp. 2469–2476, 2008.

[71] A. Fick, "Ueber diffusion," *Annalen der Physik*, vol. 170, no. 1, pp. 59–86, 1855.

[72] A. France-Lanord, Y. Wang, T. Xie, J. A. Johnson, Y. Shao-Horn, and J. C. Grossman, "Effect of chemical variations in the structure of poly (ethylene oxide)-based polymers on lithium transport in concentrated electrolytes," *Chemistry of Materials*, vol. 32, no. 1, pp. 121–126, 2019.

[73] D. M. Pesko, K. Timachova, R. Bhattacharya, M. C. Smith, I. Villaluenga, J. Newman, and N. P. Balsara, "Negative transference numbers in poly (ethylene oxide)-based electrolytes," *Journal of The Electrochemical Society*, vol. 164, no. 11, p. E3569, 2017.

[74] H.-K. Kim, N. P. Balsara, and V. Srinivasan, "Continuum description of the role of negative transference numbers on ion motion in polymer electrolytes," *Journal of The Electrochemical Society*, vol. 167, no. 11, p. 110559, 2020.

[75] M. Gouverneur, F. Schmidt, and M. Schönhoff, "Negative effective li transference numbers in li salt/ionic liquid mixtures: does li drift in the "wrong" direction?," *Physical Chemistry Chemical Physics*, vol. 20, no. 11, pp. 7470–7478, 2018.

[76] Y. Shao, H. Gudla, D. Brandell, and C. Zhang, "Transference number in polymer electrolytes: Mind the reference-frame gap," *Journal of the American Chemical Society*, vol. 144, no. 17, pp. 7583–7587, 2022.

[77] B. Hess, "Determining the shear viscosity of model liquids from molecular dynamics simulations," *The Journal of chemical physics*, vol. 116, no. 1, pp. 209–217, 2002.

[78] D. Evans and G. Morriss, "Computer phys. rep. 1, 297 (1984). 25 dj evans and gp morris," *Statistical Mechanics of Nonequilibrium Liquids*, 1990.

[79] R. Zwanzig, "Time-correlation functions and transport coefficients in statistical mechanics," *Annual Review of Physical Chemistry*, vol. 16, no. 1, pp. 67–102, 1965.

[80] T. Chen, B. Smit, and A. T. Bell, "Are pressure fluctuation-based equilibrium methods really worse than nonequilibrium methods for calculating viscosities?," *The Journal of chemical physics*, vol. 131, no. 24, 2009.

[81] A. Agrawal, D. Perahia, and G. S. Grest, "Cluster morphology-polymer dynamics correlations in sulfonated polystyrene melts: computational study," *Physical review letters*, vol. 116, no. 15, p. 158001, 2016.

[82] N. S. Gupta, K.-S. Lee, and A. Labouriau, "Tuning thermal and mechanical properties of polydimethylsiloxane with carbon fibers," *Polymers*, vol. 13, no. 7, p. 1141, 2021.

[83] D. Bresser, S. Lyonnard, C. Iojoiu, L. Picard, and S. Passerini, "Decoupling segmental relaxation and ionic conductivity for lithium-ion polymer electrolytes," *Molecular Systems Design & Engineering*, vol. 4, no. 4, pp. 779–792, 2019.

[84] J. Companik and S. Bidstrup, "The viscosity and ion conductivity of polydimethylsiloxane systems: 2. ion concentration effects," *Polymer*, vol. 35, no. 22, pp. 4834–4841, 1994.

[85] M. B. H. Othman, M. R. Ramli, L. Y. Tyng, Z. Ahmad, and H. M. Akil, "Dielectric constant and refractive index of poly (siloxane–imide) block copolymer," *Materials & Design*, vol. 32, no. 6, pp. 3173–3182, 2011.

[86] K. D. Fong, J. Self, B. D. McCloskey, and K. A. Persson, "Ion correlations and their impact on transport in polymer-based electrolytes," *Macromolecules*, vol. 54, no. 6, pp. 2575–2591, 2021.

[87] D. Qi, K. Zhang, G. Tian, B. Jiang, and Y. Huang, "Stretchable electronics based on pdms substrates," *Advanced Materials*, vol. 33, no. 6, p. 2003155, 2021.

[88] J. Pignanelli, Z. Qian, X. Gu, M. J. Ahamed, and S. Rondeau-Gagné, "Modulating the thermomechanical properties and self-healing efficiency of siloxane-based soft polymers through metal–ligand coordination," *New Journal of Chemistry*, vol. 44, no. 21, pp. 8977–8985, 2020.

[89] J. Pignanelli, B. Billet, M. Straeten, M. Prado, K. Schlingman, M. J. Ahamed, and S. Rondeau-Gagné, "Imine and metal–ligand dynamic bonds in soft polymers for autonomous self-healing capacitive-based pressure sensors," *Soft Matter*, vol. 15, no. 38, pp. 7654–7662, 2019.

[90] K. Yuan, H. Bian, Y. Shen, B. Jiang, J. Li, Y. Zhang, H. Chen, and J. Zheng, "Coordination number of li+ in nonaqueous electrolyte solutions determined by molecular rotational measurements," *The Journal of Physical Chemistry B*, vol. 118, no. 13, pp. 3689–3695, 2014.

[91] N. Ueno, T. Wakabayashi, and Y. Morisawa, "Determining the coordination number of li+ and glyme or poly (ethylene glycol) in solution using

attenuated total reflectance-far ultraviolet spectroscopy," *Analytical Sciences*, p. 19C011, 2019.

[92] S. Plimpton, "Fast parallel algorithms for short-range molecular dynamics," *Journal of computational physics*, vol. 117, no. 1, pp. 1–19, 1995.

[93] U. Olsher, R. M. Izatt, J. S. Bradshaw, and N. K. Dalley, "Coordination chemistry of lithium ion: a crystal and molecular structure review," *Chemical reviews*, vol. 91, no. 2, pp. 137–164, 1991.

[94] W. Humphrey, A. Dalke, and K. Schulten, "Vmd: visual molecular dynamics," *Journal of molecular graphics*, vol. 14, no. 1, pp. 33–38, 1996.

[95] A. Eisenberg, "Clustering of ions in organic polymers. a theoretical approach," *Macromolecules*, vol. 3, no. 2, pp. 147–154, 1970.

[96] O. Borodin and G. D. Smith, "Mechanism of ion transport in amorphous poly (ethylene oxide)/litfsi from molecular dynamics simulations," *Macromolecules*, vol. 39, no. 4, pp. 1620–1629, 2006.

[97] Y.-L. Rao, V. Feig, X. Gu, G.-J. Nathan Wang, and Z. Bao, "The effects of counter anions on the dynamic mechanical response in polymer networks crosslinked by metal–ligand coordination," *Journal of Polymer Science Part A: Polymer Chemistry*, vol. 55, no. 18, pp. 3110–3116, 2017.

[98] F. Wohde, M. Balabajew, and B. Roling, "Li+ transference numbers in liquid electrolytes obtained by very-low-frequency impedance spectroscopy at variable electrode distances," vol. 163, no. 5, p. A714. Publisher: IOP Publishing.

[99] S. Zugmann, M. Fleischmann, M. Amereller, R. M. Gschwind, H. D. Wiemhöfer, and H. J. Gores, "Measurement of transference numbers for

lithium ion electrolytes via four different methods, a comparative study," *Electrochimica Acta*, vol. 56, no. 11, pp. 3926–3933, 2011.

[100] F. Wohde, M. Balabajew, and B. Roling, "Li+ transference numbers in liquid electrolytes obtained by very-low-frequency impedance spectroscopy at variable electrode distances," *Journal of The Electrochemical Society*, vol. 163, no. 5, p. A714, 2016.

[101] J. Mindemark, M. J. Lacey, T. Bowden, and D. Brandell, "Beyond peo—alternative host materials for li+-conducting solid polymer electrolytes," *Progress in Polymer Science*, vol. 81, pp. 114–143, 2018.

[102] M. Forsyth, V. Payne, M. Ratner, S. De Leeuw, and D. Shriver, "Molecular dynamics simulations of highly concentrated salt solutions: Structural and transport effects in polymer electrolytes," *Solid State Ionics*, vol. 53, pp. 1011–1026, 1992.

[103] L. Xie and G. Farrington, "Molecular mechanics and dynamics simulation of poly (ethylene oxide) electrolytes," *Solid State Ionics*, vol. 53, pp. 1054–1058, 1992.

[104] Z. Hu and F. M. Kerton, "Room temperature aerobic oxidation of alcohols using cubr2 with tempo and a tetradentate polymer based pyridyl-imine ligand," *Applied Catalysis A: General*, vol. 413, pp. 332–339, 2012.

[105] M. Rubinstein, R. H. Colby, *et al.*, *Polymer physics*, vol. 23. Oxford university press New York, 2003.

[106] R. McNeill, R. Siudak, J. Wardlaw, and D. Weiss, "Electronic conduction in polymers. i. the chemical structure of polypyrrole," *Australian Journal of Chemistry*, vol. 16, no. 6, pp. 1056–1075, 1963.

[107] J. McGinness, P. Corry, and P. Proctor, "Amorphous semiconductor switching in melanins," *Science*, vol. 183, no. 4127, pp. 853–855, 1974.

[108] H. Shirakawa, E. J. Louis, A. G. MacDiarmid, C. K. Chiang, and A. J. Heeger, "The electronic structures of-polyacetylene," *J. Chem. Soc., Chem. Comm*, vol. 16, p. 578, 1977.

[109] J. Burroughes, C. Jones, and R. Friend, "New semiconductor device physics in polymer diodes and transistors," *nature*, vol. 335, no. 6186, pp. 137–141, 1988.

[110] Y. Hou, Y. Zhou, L. Yang, Q. Li, Y. Zhang, L. Zhu, M. A. Hickner, Q. Zhang, and Q. Wang, "Flexible ionic diodes for low-frequency mechanical energy harvesting," *Advanced Energy Materials*, vol. 7, no. 5, p. 1601983, 2017.

[111] J.-H. Han, K. B. Kim, H. C. Kim, and T. D. Chung, "Ionic circuits based on polyelectrolyte diodes on a microchip," *Angewandte Chemie International Edition*, vol. 48, no. 21, pp. 3830–3833, 2009.

[112] J.-H. Han, K. B. Kim, J. H. Bae, B. J. Kim, C. M. Kang, H. C. Kim, and T. D. Chung, "Ion flow crossing over a polyelectrolyte diode on a microfluidic chip," *Small*, vol. 7, no. 18, pp. 2629–2639, 2011.

[113] Y. Wang, Z. Wang, Z. Su, and S. Cai, "Stretchable and transparent ionic diode and logic gates," *Extreme Mechanics Letters*, vol. 28, pp. 81–86, 2019.

[114] Y. Zhang, C. K. Jeong, J. Wang, X. Chen, K. H. Choi, L.-Q. Chen, W. Chen, Q. Zhang, and Q. Wang, "Hydrogel ionic diodes toward harvesting ultralow-frequency mechanical energy," *Advanced Materials*, vol. 33, no. 36, p. 2103056, 2021.

[115] K. Nyamayaro, V. Triandafilidi, P. Keyvani, J. Rottler, P. Mehrkhodavandi, and S. G. Hatzikiriakos, "The rectification mechanism in polyelectrolyte gel diodes," *Physics of Fluids*, vol. 33, no. 3, 2021.

[116] V. Triandafilidi, S. G. Hatzikiriakos, and J. Rottler, "Poisson–boltzmann modeling and molecular dynamics simulations of polyelectrolyte gel diodes in the static regime," *Soft Matter*, vol. 16, no. 4, pp. 1091–1101, 2020.

[117] V. Triandafilidi, S. G. Hatzikiriakos, and J. Rottler, "Molecular simulations of the piezoionic effect," *Soft Matter*, vol. 14, no. 30, pp. 6222–6229, 2018.

[118] H. Li, A. Erbas, J. Zwanikken, and M. Olvera de la Cruz, "Ionic conductivity in polyelectrolyte hydrogels," *Macromolecules*, vol. 49, no. 23, pp. 9239–9246, 2016.

[119] H. J. Berendsen, D. van der Spoel, and R. van Drunen, "Gromacs: A message-passing parallel molecular dynamics implementation," *Computer physics communications*, vol. 91, no. 1-3, pp. 43–56, 1995.

[120] D. Van Der Spoel, E. Lindahl, B. Hess, G. Groenhof, A. E. Mark, and H. J. Berendsen, "Gromacs: fast, flexible, and free," *Journal of computational chemistry*, vol. 26, no. 16, pp. 1701–1718, 2005.

[121] S. Pronk, S. Páll, R. Schulz, P. Larsson, P. Bjelkmar, R. Apostolov, M. R. Shirts, J. C. Smith, P. M. Kasson, D. Van Der Spoel, *et al.*, "Gromacs 4.5: a high-throughput and highly parallel open source molecular simulation toolkit," *Bioinformatics*, vol. 29, no. 7, pp. 845–854, 2013.

[122] F. Grünewald, R. Alessandri, P. C. Kroon, L. Monticelli, P. C. Souza, and S. J. Marrink, "Polyply; a python suite for facilitating simulations

of macromolecules and nanomaterials," *Nature Communications*, vol. 13, no. 1, p. 68, 2022.

[123] S. J. Marrink, H. J. Risselada, S. Yefimov, D. P. Tieleman, and A. H. De Vries, "The martini force field: coarse grained model for biomolecular simulations," *The journal of physical chemistry B*, vol. 111, no. 27, pp. 7812–7824, 2007.

[124] M. Vögele, C. Holm, and J. Smiatek, "Coarse-grained simulations of polyelectrolyte complexes: Martini models for poly (styrene sulfonate) and poly (diallyldimethylammonium)," *The Journal of chemical physics*, vol. 143, no. 24, 2015.

[125] S. O. Yesylevskyy, L. V. Schäfer, D. Sengupta, and S. J. Marrink, "Polarizable water model for the coarse-grained martini force field," *PLoS computational biology*, vol. 6, no. 6, p. e1000810, 2010.

[126] T. Başтuğ and S. Kuyucak, "Temperature dependence of the transport coefficients of ions from molecular dynamics simulations," *Chemical physics letters*, vol. 408, no. 1-3, pp. 84–88, 2005.

[127] R. Kubo, "The fluctuation-dissipation theorem," *Reports on progress in physics*, vol. 29, no. 1, p. 255, 1966.

[128] R. Kubo, "Statistical-mechanical theory of irreversible processes. i. general theory and simple applications to magnetic and conduction problems," *Journal of the physical society of Japan*, vol. 12, no. 6, pp. 570–586, 1957.